Chapter 8

Tracers in Physiological Systems Modeling

Joseph C. Anderson and James B. Bassingthwaighte

Metabolic events within cells are intimately linked with the external influences of substrate delivery and metabolite removal. These influences include the level of cellular activity, local blood flow, transmembrane transport rates, and humoral and neural regulation of receptors and reaction rates. The question "What are the basic principles that the developers of tracer models should use?" evokes discussion on the scope of the modeling: an extreme is "minimal modeling," wherein one considers only the observations of the injected tracer-labeled solute itself (as in pharmacokinetics), its reaction products, or its effects on the physiology (as in pharmacodynamics). Minimal modeling can work for classification or diagnosis, but unless the model has the depth to encompass mechanisms of tracer handling, it doesn't often provide an explanation of the mechanisms. A two compartment model with a binding site illustrates that recognition of the anatomic constraints would foster a better understanding of the system kinetics. Another example is to abandon the lumped compartmental representation of spatially extended capillary-tissue exchange in favor of using anatomic-based equations, thereby obtaining physically meaningful estimates of parameter values. Consequently, we advocate adherence to a broad set of principles for the design and application of models to the understanding of physiological systems: (1) consider the anatomy (a biological constraint) as an essential part of the data, (2) take into account the background physiological state of the subject (biochemical, thermodynamic constraints), (3) consider the processes that the tracer labeled solutes undergo (mechanisms of transport and reaction), (4) be obedient to the laws of physics and chemistry (conservation principles for mass, energy, charge, momentum, etc.), and (5) adhere to a set of modeling standards to allow reproducibility and dissemination of the model.

Introduction

Advances in computational speed and simulation interface technology now make it practical to choose valid physiological modeling approaches rather than using minimal models for classification or description. Here we will argue that by following a few general guidelines and standard scientific ideas one can bring additional power, reliability, and accuracy in parameterization, and, best of all, improved insight into the processes involving solute transport.

The "principles" are a combination of scientific principles and psychological aids or perspectives that make it easier to keep focused. Here we address the users of "compartmental analysis" because it appears that the nomenclature and computational toolkits commonly used are compromising the efficacy of this particular community of skilled scholars in determining mechanisms to explain the observed kinetics. These inefficiencies exist in spite of Berman's (1) classic article on modeling which clearly espoused properly principled modeling, including examination of underlying assumptions. While making this bold general criticism, we recognize that there is an immense amount of productive contributory work accomplished with the same tool kit that we are criticizing. At the same time, we suggest using an alternative methodology that forces adherence to scientific principles and facilitates placing particular tracer models into the context of discovery science, specifically, to attempt to elucidate biological mechanisms in networks of processes, going beyond the kinetics.

Integrative modeling is only beginning. Each of the thousands of models in existence is potentially a component module in a larger scale integrated model. Model archiving and public accessibility will make it possible for future investigators to combine modules, thereby constraining the behavior of the individual components. It is therefore contributory to the community effort to make each model available, understandable, reproducible, verifiable and to provide along with it the data that demonstrates its validity with respect to the biology. Here, we will focus on two types of compartmental analysis, which are frequently used inappropriately in that they may not conform to physical and physiological constraints.

The first model discussed is a two-compartmental system that is rendered complicated because one compartment contains a buffer system. Each compartment in the system is considered as lacking spatial gradients meaning they are "well-mixed," "lumped," "compartmental," or "stirred tank." Therefore, each can be described using an ordinary differential equation (ODE). A common example occurs when describing the kinetics of exchange and metabolism. These models are based on the idea that a solute (drug, substrate or metabolite, receptor, enzyme, etc.) can be treated as being within a lumped system, i.e. one wherein the concentration of the solute is everywhere uniform.

For almost a century, errors resulting from using well-mixed compartmental analysis have been obvious to those examining oxygen exchange. Krogh (2) with Erlang modeled oxygen profiles in capillary tissue exchange units. They showed that

if the tissue oxygen consumption was uniform, there were nearly exponential gradients in oxygen tension, P_{O2}, along the capillary length, and parabolic profiles in P_{O2} in the tissue between capillaries. For this case and other similar cases spatial gradients are significant and partial differential equations (PDEs) must be used.

In this essay we argue that using PDEs is as simple conceptually as using ODEs. One of the reasons for using ODEs which assumes stirred tank representation (compartmental models) was to reduce computation time, a goal rendered less critical with fast modern computers, but important when one has to optimize model predictions to fit many data sets. With modern numerical techniques, PDEs can be solved very quickly. Modern simulation systems analysis tools makes PDE usage in practice as easy as using ODEs. PDEs are required to obtain physically correct measures of system parameters. The argument is simple: the use of incorrect representation of the anatomy of the system causes artifactual errors in parameter estimates for transport rates and reaction rates.

Approaches and Methods

Definition of tracer, C*

The advantage of using tracers is that nonlinear processes are rendered linear when the overall system is in steady state for all solutes except the tracer itself. The addition of tracer does not perturb the steady state but allows the determination of rate constants within the system for the particular steady state. The rationale for this is that the concentration of the tracer-labeled solute C* is in negligible concentration compared to that of the tracee or mother substance, C, so that changes in C* have no impact on the kinetics for the tracee.

For the transport of C, the rate constant depends on its concentration *C*, for example, relative to the dissociation constant for the process of binding to the transporter:

$$\frac{dC}{dt} = -k(C) \cdot C \qquad [1]$$

where *C* is a concentration, M, *k*(*C*) is a transfer or reaction rate, s^{-1}, which is a function of the concentration of *C*. When tracer, C*, is transported by the same process as the tracee, then the transport of *C* + *C** is essentially the same as that for *C* alone and the transport of *C** is given by:

$$\frac{dC^*}{dt} = -k\left(C + C^*\right) \cdot C \qquad [2]$$

By definition, tracer concentrations are $C^*/C \ll 1$ and usually $< 1/10^{12}$. As a result, $k(C+C^*) = k(C)$ and $k(C)$ is independent of C^*, and

$$\frac{dC^*}{dt} = -k\left(C\right) \cdot C^* \qquad [3]$$

showing that the rate constant for C^* is identical to that for the tracee C, at the particular concentration, C, in steady state. When the concentration of C is slowly varying then the same considerations apply, but in that case $k(C)$ becomes $k(C(t))$. Likewise, when C varies spatially within a capillary-tissue exchange region, *i.e., $C(x,t)$* is a function of position x, then this rate is expressed as $k(C(x,t))$.

Writing dual models for tracee and tracer together

Most tracer models are developed from node/edge relationships in networks of reacting species and then written in the form of linear sets of ordinary differential equations. This methodology is based on two independent assumptions: (a) that a node, the compartment, represents a time-dependent variable that is spatially uniform, as if concentrations are instantaneously mixed over a finite space, and (b) that the edges, the rate processes, have linear, constant coefficients for tracer because the mother or tracee system is in a constant, non-oscillating steady state. We will explore the effects of deviations from these assumed conditions.

When (b) is applicable, then the rate coefficients for tracer can be considered linear and constant at each location in the system, though they are necessarily different in each location whenever the concentration of tracee is different. A reliable way to approach the analysis of such a system is to model tracee and tracer together before jumping to the linearized tracer equations.

As a first example, to make the assumptions clear, we discuss a two compartment system, first for mother substance, tracee, and then for tracer. The second example will be a flow-through system, comprised of blood and tissue.

Modeling of a Two-Compartment System

Model 1A: Non-instantaneous binding (equivalent to a 3 compartment system)

This section focuses on the effects of solute binding on volumes of distribution, on exchange rates and times to equilibration, and on the estimation of physiological parameters.
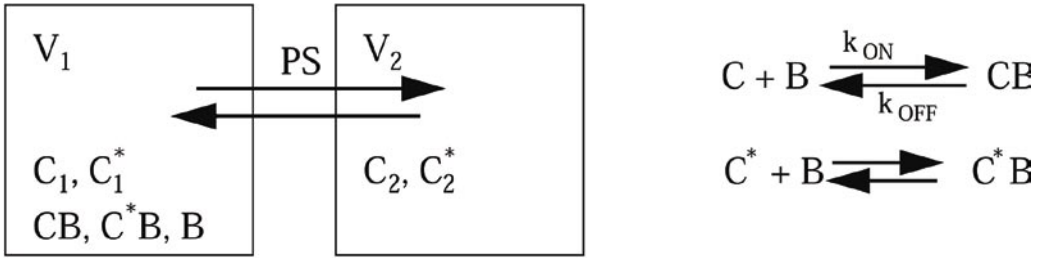
Figure 8.1. A two compartment system for the passive exchange of solute C between the stirred tanks. In tank 1 the solute may bind with a ligand B whose total concentration is B_T, mM, in accord with the reaction shown at right. The reaction rates for tracer C* are determined by the concentration C of tracee or mother solute. PS, ml s⁻¹, is a conductance, the permeability-surface area product of the membrane separating the two chambers, allowing bidirectional passive flux.

Model I: Binding site in compartment 1 of a 2-compartment system, Tracee

This system is diagrammed in Figure 8.1. For this system the equations are

$$\frac{dC_1}{dt} = -\frac{PS}{V_1}\left(C_1 - C_2\right) - k_{ON} \cdot B \cdot C_1 + k_{OFF} \cdot CB \qquad [4]$$

$$\frac{dCB}{dt} = k_{ON} \cdot B \cdot C_1 - k_{OFF} \cdot CB \qquad [5]$$

$$B = B_T - CB \qquad [6]$$

$$\frac{dC_2}{dt} = \frac{PS}{V_2}\left(C_1 - C_2\right) \qquad [7]$$

where C is concentration of tracee, mM; t is time, seconds; PS is a passive conductance, a permeability-surface area product, cm s⁻¹ multiplied by cm², or ml s⁻¹; V_1, ml, is the volume of compartment 1; k_{ON}, mM⁻¹s⁻¹, is the rate of binding of C to the ligand B within compartment 1 to form CB, and k_{OFF}, s⁻¹, is the rate of release of C from CB, so the dissociation constant, $K_D = k_{OFF}/k_{ON}$, mM, and B_T, mM, is the total concentration of ligand (bound + free); C_2, mM, is the concentration in compartment 2 whose volume is V_2, ml.

To illustrate the behavior of this model, B_T = 1 mM, K_D = 0.1 mM and solute is introduced into the system at an initial value of C_1=1 mM. The results are shown in Figure 8.2 for various values of k_{ON}.

Because binding is slow relative to permeation, there is a rapid early overshoot in C_2 and a slow return to the final equilibrium condition where K_D =B•C_1/CB.
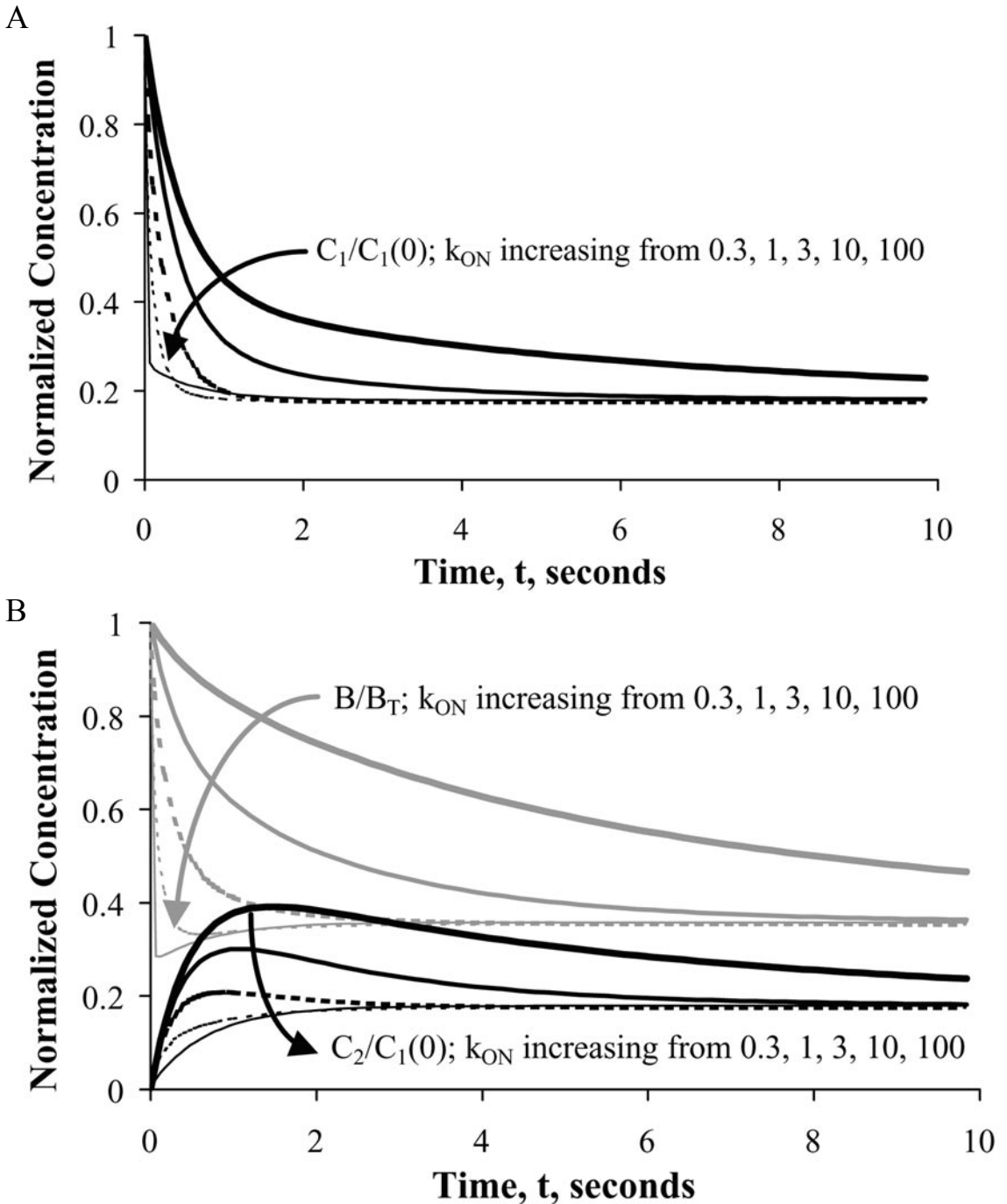
A

B

Figure 8.2. Equilibration of C across a barrier with a binding ligand in V_1 for increasing values of k_{ON} from 0.3 to 100 mM^{-1}s^{-1}. Panel A: The initial concentration C_1 was as if 1 μmole of C were injected into a volume V_1 = 1 ml at t = 0. Parameters were PS = 1 ml/s, B_T = 1 mM, K_D is constant at 0.1 mM, and V_2 = 1 ml. Panel B: Concentrations of free binding sites, B, and of C_2.

Model 1B: Instantaneous binding of solute to ligand in Compartment 1: This is a reduced form of Model 1A assuming that the binding of C to any free B occurs instantaneously. When both k_{OFF} and k_{ON} are rapid CB can be calculated algebraically instead of using a differential equation. Using Eq. [5] and setting the derivative to zero to represent the equilibrium between C and CB, then

$$\frac{dCB}{dt} = 0 = k_{ON} \cdot B \cdot C_1 - k_{OFF} \cdot CB \qquad [8]$$

$$K_D = \frac{k_{OFF}}{k_{ON}} = \frac{B \cdot C_1}{CB} \qquad [9]$$

and

$$\frac{d(C_1 + CB)}{dt} = -\frac{PS}{V_1}(C_1 - C_2) \qquad [10]$$

CB is defined by substitution of Eq. [6] into Eq. [9]:

$$CB = (B \cdot C_1)/K_D = ((B_T - CB) \cdot C_1)/K_D$$

Solving for CB by rearranging the expression above gives an algebraic expression for CB independent of free B:

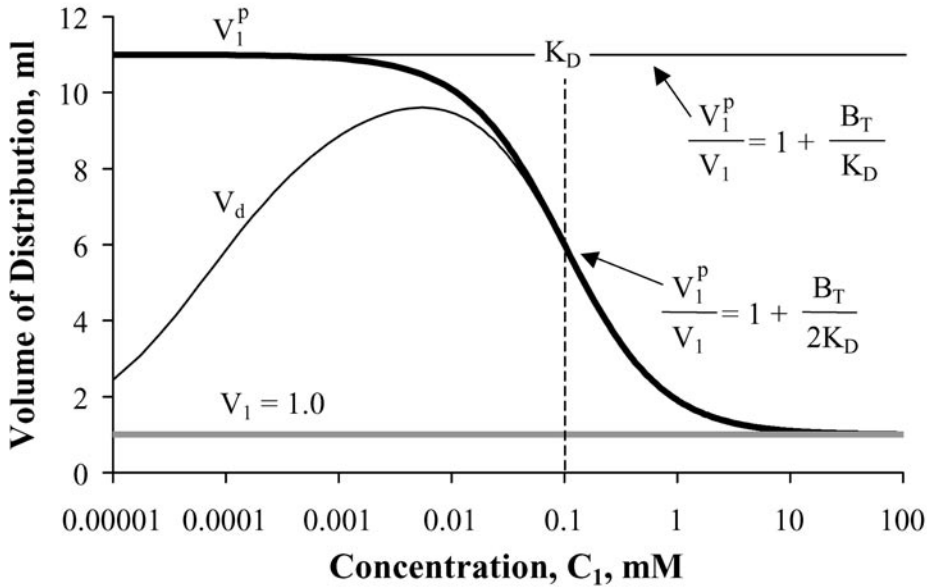$$CB = \frac{B_T \cdot C_1}{K_D + C_1} \qquad [11]$$

The equilibrium relationship between CB and C_1 can be substituted into the left hand side of Eq. 10 and after differentiation gives

$$\frac{dC_1}{dt}\left(1 + \frac{B_T}{K_D + C_1} - \frac{B_T \cdot C_1}{(K_D + C_1)^2}\right) = -\frac{PS}{V_1}(C_1 - C_2) \qquad [12]$$

Now it can be seen that the theoretical volume of distribution is not V_1 but a larger volume, V_1^P. The quadratic term is not relevant when C_1 is constant. Then, V_1^P can be seen to be a concentration-dependent volume of distribution at <u>equilibrium</u>:

$$V_1^P = V_1\left(1 + \frac{B_T}{K_D + C_1}\right) \qquad [13]$$
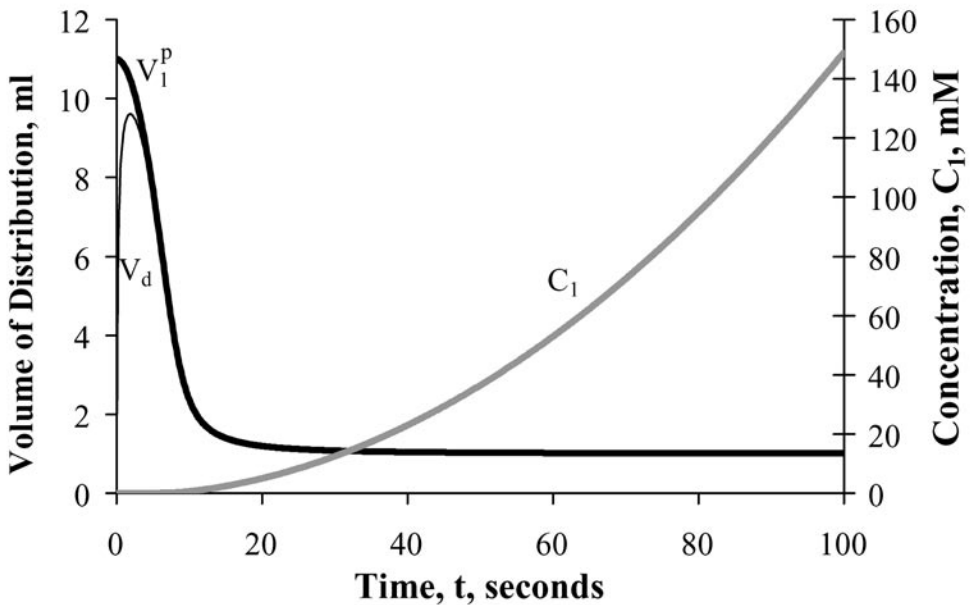
A

B

Figure 8.3. Panel A. Volumes of distribution, V_1^p (Eq. [13], for equilibrium binding) and V_d (Eq. [14], for slow binding) versus concentration C_1. Panel B. The in silico experiment was to raise the concentration C_1 at an accelerating rate into a stirred tank of volume V_1=1.0 ml (panel A). Conditions were: K_D = 0.1 mM; k_{ON} = 100 mM^{-1}s^{-1}; and PS = 0. The rate of concentration increase in V_1 was 30 nM s^{-2}, such that after 20 seconds C_1 has reached 5 mM. The theoretical V_1^p (thick black line) can be seen to diminish in accord with Eq. 13 as C_1 rises. The actual or effective V_d = V_1(1 + CB/C_1). V_d is initially equal to V_1 because CB is zero (off left-side of graph). Then CB rises rapidly as binding occurs to form CB (panel B), but in spite of the fairly high k_{ON}, CB does not reach the equilibrium binding level V_1^p until about 5 seconds have passed at which point V_d =V_1^p.

Now Eq. [12] can be rewritten:

$$\frac{dC_1}{dt} = -\frac{PS}{V_1^P}(C_1 - C_2) \qquad [14]$$

Now the system equations define C_1 by Eq. [14] (with Eq. [13]), C_2 by Eq. [7] (unchanged), and 2-compartments using a modified, concentration-dependent volume of distribution. Plotting V_1^P versus C_1 (Figure 8.3) shows that the maximum V_1^P is at any $C_1 < K_D$ where most of the solute is bound and is $V_1(1 + B_T/K_D)$. When $C_1 = K_D$, half of B_T is bound and $CB = B$. At high concentrations much greater than K_D, all the binding sites are filled and V_1^P goes to V_1. In this example with $B_T/K_D = 10$, the maximum volume of distribution V_1^P is 11, and is observed when equilibrium is attained at low concentrations.

However, when the solute does not arrive at the binding site instantly or does not react instantaneously, the effective volume of distribution V_d must be less. V_d in a transient situation is defined by the actual concentration CB as determined from Model 1A (Eq. [5]). CB augments the free concentration, C_1, so

$$V_d = V_1 \left(1 + \frac{CB(t)}{C_1(t)} \right) \qquad [15]$$

This is shown by the thin black curve in Figure 8.3 for which the binding rate is moderately high, $k_{ON} = 100$ mM^{-1}s^{-1}. This causes a lag in the rise of the effective volume of distribution when C_1 is rising (bottom panel of Figure 8.3.) During a rising (falling) transient, the maximum V_d is less (more) than that expected with instantaneous binding, V_1^P.

Model 1.C: Tracer added to a slow binding system in equilibrium for tracee. The phrase slow binding (and slow release) implies that k's are similar to PS/V_1^P. Tracer concentrations are C_1^* and C_2^*. The tracer equations take their coefficients from the tracee, and the equations are the same as for the tracee, Eqs. [4] to [7]:

$$\frac{dC_1^*}{dt} = -\frac{PS}{V_1}(C_1^* - C_2^*) - k_{ON} \cdot B \cdot C_1^* + k_{OFF} \cdot C^*B \qquad [16]$$

$$\frac{dC^*B}{dt} = k_{ON} \cdot B \cdot C_1^* - k_{OFF} \cdot C^*B \qquad [17]$$

$$B = B_T - CB - C^*B \qquad [18]$$

and

$$\frac{dC_2^*}{dt} = \frac{PS}{V_2}\left(C_1^* - C_2^*\right)$$

[19]

where Eq. [18] for free B gives the same value as from Eq. [6] since the concentration of C^*B is negligible. The conductance PS is here considered purely passive, involving no transporter.

Figure 8.4 shows the effect of adding tracer to the system after equilibration of tracee has occurred between the two chambers and between free and bound forms in V_1. The shape of the relaxation curve for C_1^*(t) in V_1 is different for increases in k_{ON} (panel B) compared to increases in PS (panel D). Increasing PS from 0.1 ml s^{-1} to higher values leads to rapid entry of C into V_2, resulting in an overshoot in C_2 above the final equilibrium value. This overshoot has the effect of actually prolonging the transient, as can be seen by comparing the tails of the tracer curves (panel D) for $PS = 0.1$ ml s^{-1} and $PS = 1.0$ ml s^{-1}, the latter converging more slowly. The reason for this is that the early loss into V_2 causing the same overshoot for C_2^* as was seen in the first few seconds for the tracee C_2, this renders it unavailable to the binding site in V_1 until after it returns to V_1 from V_2. Mechanistic modeling of this sort reveals phenomena that are not intuitively obvious. This would not be evident in straightforward compartmental modeling with constant coefficients.

Model 1.D: Instantaneous Versus Slow Tracer Binding in Tracee Steady State Situations

When binding is instantaneous the effective volume of distribution for tracer is determined solely by the steady state concentrations of tracee and binding ligand:

$$\frac{dC_1^*}{dt} = -\frac{PS}{V_1} \cdot \frac{\left(C_1^* - C_2^*\right)}{\left(1 + B_T/\left(K_D + C_1 + C_1^*\right)\right)} = -\frac{PS\left(C_1^* - C_2^*\right)}{V_1^P}$$

[20]

where C_1 in the denominator denotes the constant tracee concentration. (Second order terms in the derivative are ignored.) Because C_1^* is orders of magnitude smaller than C_1 (the definition of a tracer), the denominator on the right side equals V_1^P as in Eq. [13]. The tracer C_2^* equation is the same as Eq. [19]. Equations are not needed for CB or B since the information is accounted for in the denominator of Eq. [20]. The coefficients in Eq. [19] and Eq. [20] are only constant when the tracee solute is in steady state. Then and only then, the tracer equations are linear, with constant coefficients. From this it seems obvious that the tracer transient equations could simply use the coefficients for the tracee; for example, if the PS for the membrane represented the conductance for a non-linear facilitating transporter, then using its value at the
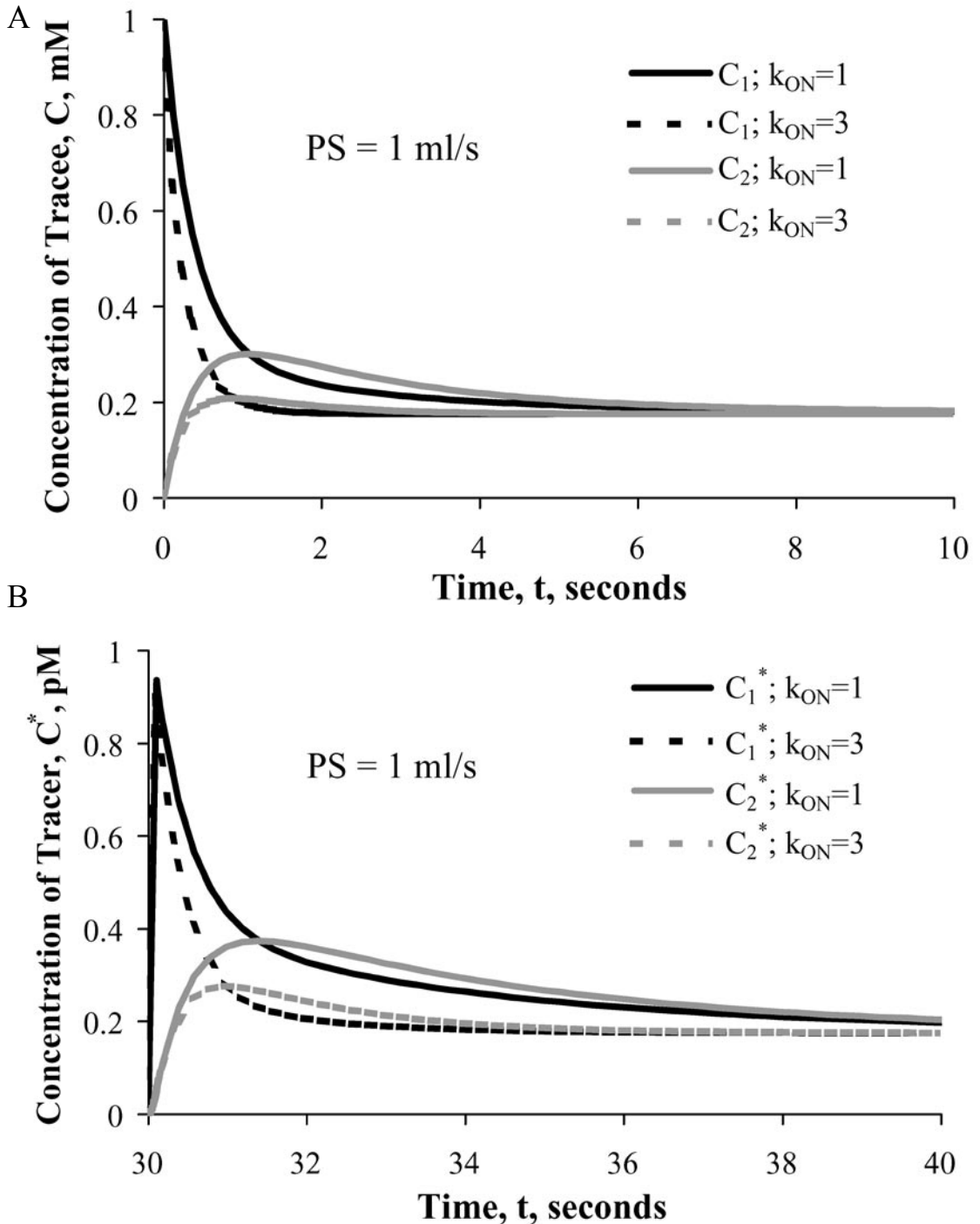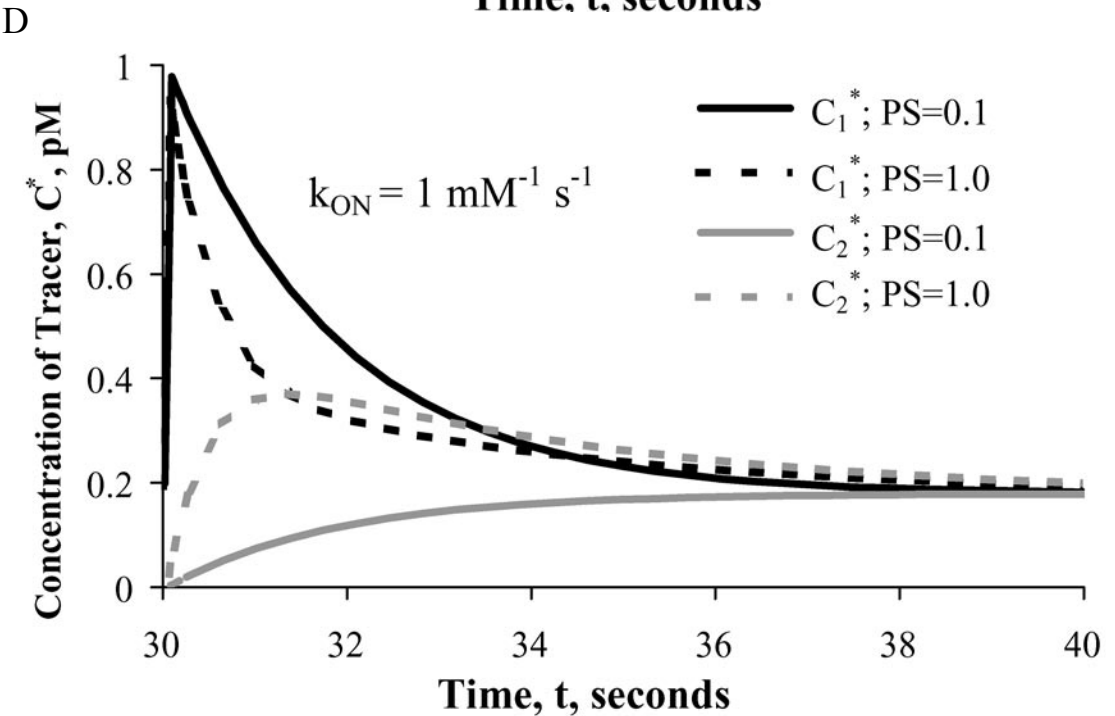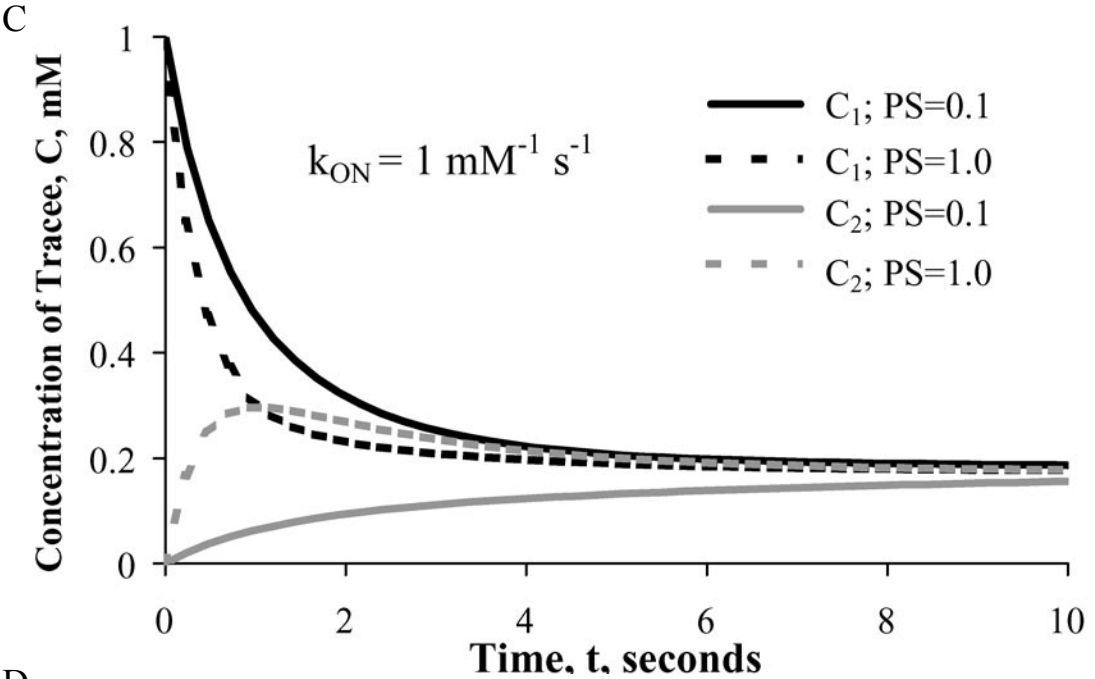
Figure 8.4. Tracer added (Panels B and D) after tracee and binding site have equilibrated (Panels A and C) with K_D=0.1 mM, B_T=1 mM, and V_1=V_2=1 mM. Curves denoting tracer transients in panels B and D follow equilibration in panels A and C. Panels A and B: With PS constant at 1 ml s^{-1}, increasing k_{ON} reduces the time for tracee (panel A) and tracer (panel B) to equilibrate. Panels C and D: With k_{ON} = 1 mM^{-1}s^{-1} and

C

D

K_D is constant, increasing PS from 0.1 to 1.0 ml s^{-1} produces a faster initial part of the tracer transient (from 30 s < t< 35 s) but the actual time to equilibration is actually lengthened, having a long low tail. For both perturbations, the overshoot in C_2 is less than the overshoot in C_2^* because of non-linear kinetics resulting from binding site disequilibrium.

particular C_1 and C_2 for the tracee in steady state would be exactly correct for the tracer in the transient. This is true for processes involving conductances but not for volumes of distribution, as will be seen by examining tracer transients for this system.

Examine the situation when k_{ON} is 10^4 mM^{-1}s^{-1}, resulting in effectively instantaneous equilibration between C_1 and B, as in Figure 8.5A. Starting from initial conditions $C_1=C_2=0$, a 1 mM pulse of C is introduced into compartment 1 and equilibrium is achieved in less than 5 seconds. At t = 10 seconds, a bolus of tracer is injected into V_1. The tracer concentrations, C_1^* and C_2^* were calculated in two ways, using equations describing slow binding, Eq. [16] to Eq. [19], and then using equations describing instantaneous binding, Eq. [19] and Eq. [20]. The results show that the two methods give identical results (within about 0.0001 mM using the solver CVODE) and that Eq. [20] is correct when the binding rate is truly fast.

Figure 8.5B illustrates the error caused by applying the instantaneous equilibrium assumption to a system with slow binding, $k_{ON} = 1$ mM^{-1}s^{-1}. Shown are the "true" tracer curves for the tracer concentrations, C_1^* (thick solid) and C_2^* (medium solid), and for C^*B (thin solid), using the slow binding model of Eq. [16] to Eq. [19]. The same three concentrations calculated from the instantaneous binding model of Eq. [19] and Eq. [20] are shown as corresponding gray dashed lines. As expected, the two models predict quite different tracer profiles. The solid lines, which account for the slow binding kinetics, display transients that are quite different from the instantaneous binding model. C_1^* now has a high early peak, as does C_2^*, but C^*B shows a slow monotonic rise to its equilibrium level. The dashed curves are unchanged from Figure 8.5A by the change in k_{ON}, of course, as the assumption for Eq. [20] is that equilibration is instantaneous.

Estimating model parameters while making the erroneous equilibrium assumption
Analyzing observed tracer data using an equilibrium (i.e., fast) binding assumption is often correct as shown in Figure 8.5A and might be considered reasonable if we hadn't been subjected to the slow binding situation presented in Figure 8.5B. Thus, it is interesting to determine what might be the parameters estimated by fitting the solid lines of Figure 8.5B, which are correct solutions, with the equilibrium-based model described by Eq. [19] and Eq. [20].

The result shown in Figure 8.6A is that the 2-equation pseudo-equilibrium model can give a good fit of C_1^* to the "data," the correct solution, shown by the thin continuous line, but at a cost. One cost is sacrificing accuracy in estimating the real kinetic parameters. Another cost, not so obvious if one only observes C_1^*, is the failure to predict C_2^* "data," closed circles, with the 2-equation psuedo-equilibrium model for C_2^* as indicated by the thick continuous line. Figure 8.6B shows how the parameters diverge from the correct values as they converge on a fit for C_1^*. The results of a set of seven optimization runs, Table 8.1, shows that the reduced model has little sensitivity to either B_T or K_D because their final values vary widely for very close fits of the "data." The estimates for *PS* are quite consistent, being about 25% higher than for the original
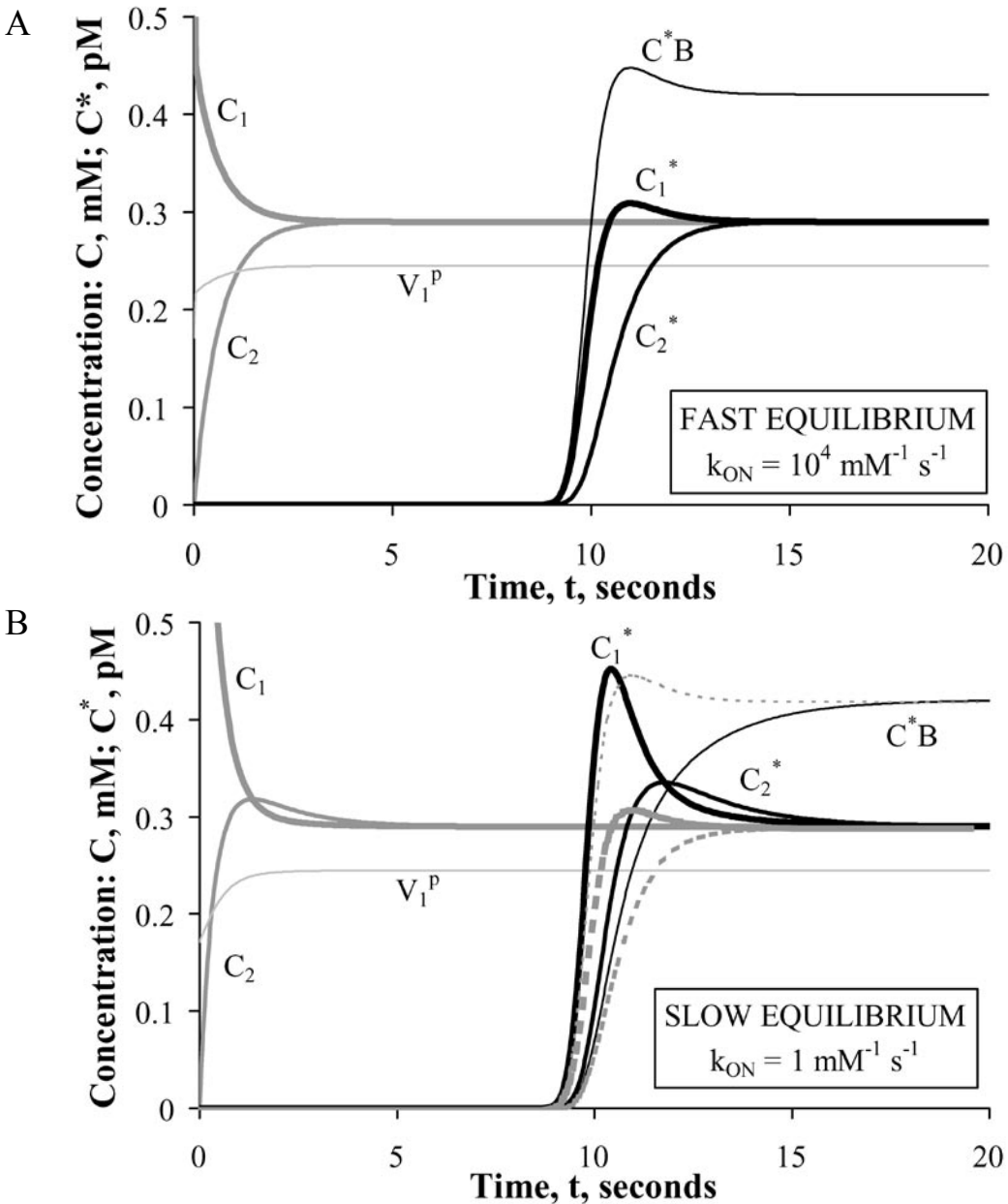
Figure 8.5. Tracer transients, C^*, when there is solute binding and permeation. Model parameters are B_T = 1 mM, K_D = 0.4 mM, $V_1 = V_2 = 1$ ml, PS = 1 ml s^{-1}. At t = 10 s, a bolus of tracer is injected into V_1 as a narrow Gaussian pulse (mean time = 10 s, standard deviation = 0.5 s). Panel A: Fast binding, $k_{ON} = 10^4$ mM^{-1} s^{-1}. Results are the same for C_1^* using either Eq. [16] or Eq. [20]. For this fast equilibration situation Eq. 20 is correct. Panel B: Slow binding, $k_{ON} = 1$ mM^{-1} s^{-1}. Results for C_1^* and C_2^* from t = 9 to t = 15 seconds using Eq. [16] to Eq. [19]. differ dramatically from those using Eq. [20] for C_1^*, showing that Eq. [20] is erroneous even though the system for mother substance is in steady state. The linearization, using an equilibrium-based coefficient in Eq. [20], is inappropriate when a capacitance is involved and that capacitance is changing more slowly during the tracer transient than is assumed for the coefficient in Eq. [20].
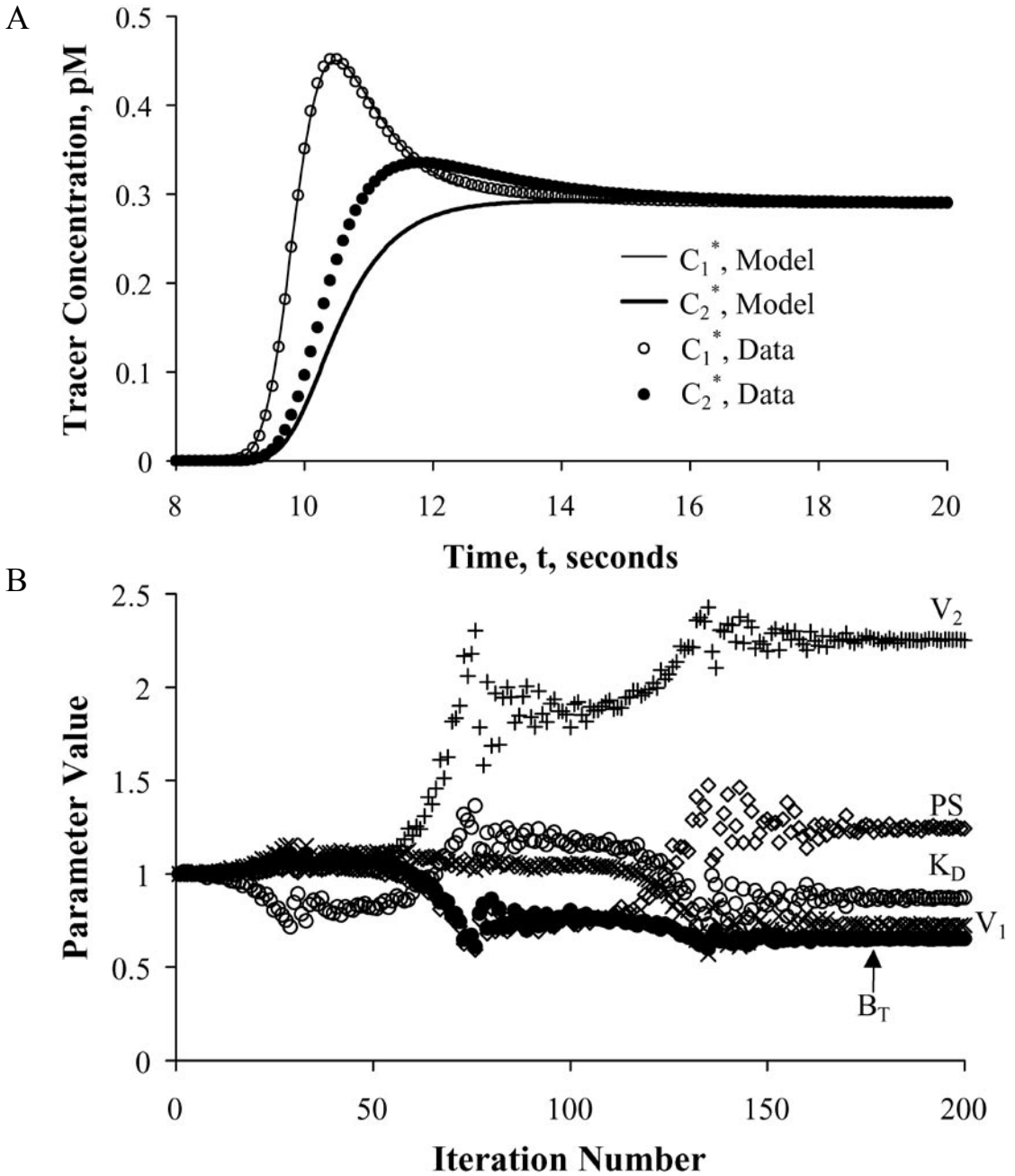
Figure 8.6. Optimization trial of the 2-equation pseudo-equilibrium model to fit C_1^* "data" on tracer transient computed using the full 3 equations. Panel A: The model curve (thin line) fits the "data" (open circles) for C_1^*, but the parameters are different. The "data" curve from the true 3-equation model C_2^* (closed circles), not included in the objective function since it would normally not be observed, is well above the model solution for reduced 2-equation model C_2^* (thick line) during the transient, though the 2-equation model is close to the correct steady state level at t = 20 s. Panel B: The optimized parameters were started at the correct values for the mother substance, and diverged to quite different values (Table 1, Trial 6) to achieve a good fit to C_1^*. See Table 1 for results of the other Trials.

Table 8.1. Results of Optimizing the 2-Eq Equilibrium Model Eq. [19] and Eq. [20] to Fit 3-Eq "Data" as show in Figure 8.6.

Parameter	*Original Values*	Trial 1	Trial 2	Trial 3	Trial 4	Trial 5	Trial 6	Trial 7
B_T	1.0 mM	0.734	0.014	0.562	0.045	0.201	0.651	2.229
K_D	0.4 mM	0.813	0.033	0.008	0.252	0.001	0.869	0.485
PS	1.0 ml s^{-1}	1.247	1.246	1.247	1.246	1.246	1.246	1.246
V_1	1.0 ml	0.671	1.116	0.038	1.073	0.483	0.723	0.230
V_2	1.0 ml	2.254	2.254	2.254	2.254	2.254	2.254	2.254
RMS Error		221.9	221.9	220.5	221.9	221.8	221.9	221.9

"data," and estimates of V_2 are consistently over twice the correct value, while estimates of V_1 are mostly low and widely scattered. However, the table reveals significant covariance amongst parameters, e.g. the low estimates of V_1 are associated with high affinity of the binding site (low values of K_D). Since it is mass or quantity that counts, when the estimated affinity, K_D, chanced to increase in the optimization, the volume of compartment 1 decreased. To compensate, compartment 2 volume increased in order to fit the downslope of the model curve after its peak and to keep the time constant of the transient of the order of V_2/PS.

Supposing that the only observable variable is $C_1{}^*$, how then could one avoid an errorneous interpretation of the configuration of the system? Since $C_1{}^*$ can be fitted nicely with a 2-compartment model, how would one know that 1) there is a binding site; and 2) the system compartmental volumes and the PS are wrongly estimated? The first part of the answer is to use other information. Are the estimates of V_1 and V_2 in accord with the known anatomy? That comparison gives a good clue if other data on V_1 and V_2 are available. The second part of the answer is that the concentration of tracee should be measured directly if possible. A second approach is to change the conditions and repeat the experiment, e.g., raise the concentration of tracee. The K_D is presumably unknown, but if the concentration happened to be raised from below to above the value of K_D, the binding site will be revealed by the reduction in apparent volume of distribution. If the original C_1 was far below the K_D, a decade increase in C_1 may not suffice to change $V_1{}^p$ but if the original C_1 was greater than about $0.01K_D$ then a diminution in $V_1{}^p$ at the raised concentration will reveal the presence of B, allow a crude estimate of B_T and K_D, and certainly provoke doing further experiments to estimate them accurately.

Another approach is to test the possibility that binding can be ignored. To do this one sets the value of B_T to zero, removes both k_{ON} or K_D from the parameters to be optimized, and proceeds to obtain a best fit of the same 2-Eq model to the 3-Eq model solution. The results in Figure 8.7 demonstrate that the fit is just as good as that using the more complete model, with the root mean square error being 221.9, comparable to

those in Table 1, but the parameters differ: V_1 is 1.159 ml, V_2 is 2.25 ml, and PS is almost unchanged at 1.245 ml s^{-1}. As before, change in apparent volumes make up for the accumulation of bound ligand in the original system. The lesson here is that an incorrect model is not necessarily going to be invalidated by comparison with a parsimonious data set that includes no information on the actual volumes in the real system. If anatomic data had defined these volumes to within 10 or 20% of the correct values then the analyst would have noted the disparity between estimated and real volumes, particularly for V_2, and would have been more likely to incorporate the binding site into the model.

The sum of the volumes multiplied by the concentrations must account for the total mass of tracer injected, even though B_T was set to zero and the final part of the curve for $C_1{}^*$ had to match that from the data where binding was included. Therefore the sum of the tracer mass in Figure 8.5 has to match the sum in Figure 8.7, i.e. $V_1 C_1{}^*$ + $V_2 C_2{}^*$ + $V_1 C_1{}^* B$ (in Fig. 8.5) = $V_1 C_1{}^*$ + $V_2 C_2{}^*$ (in Fig. 8.7), which is exact. In Figure 8.5 final values of $C_1{}^*$ and $C_2{}^*$ were both 0.29 x 10^5 pM and $C_1{}^* B$ was 0.42 x 10^5 pM for a total of 10^5 pmole. In Figure 8.7 the total estimated volume is 3.41 ml and the final concentration is 0.293 x 10^5 pM giving a total of 10^5 pmole injected and retained in the system. Mass is conserved! Cobelli et al (3) make this point succinctly, and further argue that using anatomic information narrows the confidence limits for parameter estimates.

The first lesson from Figure 8.7 is that the data can be fitted without any consideration of either binding or of anatomical constraints, but ALL of the parameter estimates were erroneous. Though the virtual volume of distribution was correct, the total anatomic water volume was overestimated by 70% and the PS by 25%. Thus linear compartmental analysis was misleading. If the K_D had been 0.1 mM, as in Figure 8.2 instead of 0.4 mM, then the errors would have been larger, as the total volume of distribution would have been 12 instead of 3.4 ml. This difference would have been observed if the tracer had been injected at two different known levels of tracee.

The second lesson from Figure 8.7 is that it is important to measure the background, native solute concentration, when doing tracer experiments in order to interpret the results in terms of the underlying physiology and biophysics. For example, when another solute is added to the system, the rate coefficient PS/V_1^p in Eq. 19 and Eq. 20 might be changed. Additionally, it may be useful to consider how one might detect or identify changes in the following: (a) PS (e.g. changing width of a channel); (b) the level of free binding sites, B (e.g. reduced by B binding to the new solute); (c) K_D (e.g. by an allosteric effect on the binding protein); (d) C_1 (e.g. by influencing some other reaction involving C in either V_1 or V_2); or (e) V_2 (e.g. by shrinking or expanding the cell volume). While this list is hardly exhaustive, the idea is to contemplate the effects of other possible influences, as a routine check.

II. Capillary-Tissue Exchange: Convention, Premeation, Reaction, and Diffusion

The two-compartment system from Figure 8.1 is here modified to incorporate flow, as shown in Figure 8.8, thus identifying V_1 as the vascular region, the membrane as the
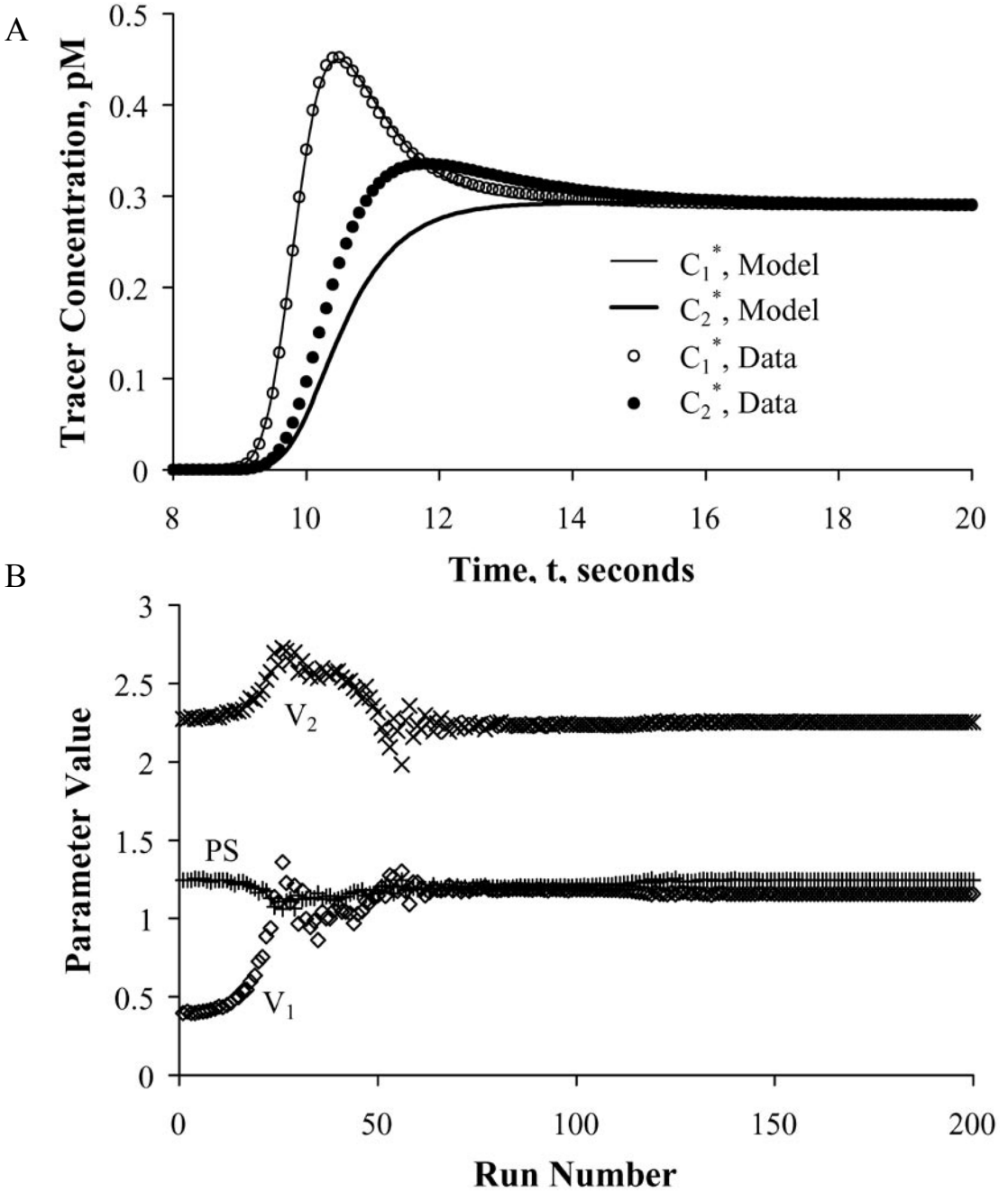
Figure 8.7. Optimization to fit the 2-Eq model to the 3-Eq model solution assuming the absence of any ligand binding in V_1 or V_2. The matching of the C_1^* data (open circles) by the 2-Eq model is as good as that in Fig 6, but the parameter values are different; the error in C_2^* is about 25% when t = 12s. Estimated values: $V_1 = 1.159$ ml, $V_2 = 2.254$ ml, and PS = 1.246 ml/s. Correct values: $V_1 = 1$ ml, $V_2 = 1$ ml, PS = 1 ml s^{-1}, $B_T = 1$ mM, and $K_D = 0.4$ mM.

capillary barrier, and V_2 as the tissue. The system is considered as a homogeneously perfused organ with constant volumes and steady flow, F, in and out. Now, in order to put it into the context of substrate delivery and metabolism, we switch to standard physiological representation of the units, defining them per gram of organ mass. F, PS, and the consumption G have units ml g^{-1} min^{-1}, and the volumes have units ml g^{-1}. This notation normalizes flows, substrate use, etc. to be independent of organ mass.

To keep the system simple so as to focus on the blood-tissue exchange, the intratissue consumption is considered to be a first order process, as if the substrate concentration is far below the K_D for an enzymatic reaction.
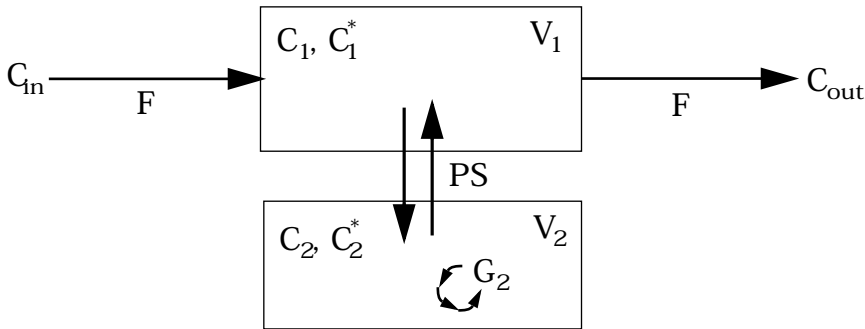

Figure 8.8. A two compartment system for the facilitated exchange of solute C between flowing blood and surrounding stagnant tissue. Solute binding in the blood is neglected in this example. Flow F, g^{-1} min^{-1}, carries in solute at concentration C$_{in}$, mM, and carries out a concentration C$_{out}$, mM. The rates of permeation or reaction for tracer C* are determined by the concentration C of tracee or mother solute. PS, ml g^{-1} min^{-1}, is a conductance, the permeability-surface area product of the membrane separating the two chambers, allowing bidirectional flux. G$_2$ ml g^{-1} min^{-1}, is a reaction rate for a transformation flux such that the product G$_2$·C$_2$ is mmole g^{-1} min^{-1}.

A technique developed to distinguish individual processes involved in blood-tissue exchange and reaction was the Multiple-Indicator Dilution (MID) technique. It was used first by Chinard (4) for the purpose of estimating the volumes of distribution for sets of tracers of differing characteristics: the mean transit time volume, $V_{mtt} = F \times \bar{t}$ where $\bar{t}$ is the mean transit time through the system. He did not estimate permeabilities as his studies were on highly permeable solutes. Crone (5) analyzed the technique, showing how it could be used to estimate PS from the outflow curves for a simultaneous injection into the inflow of a solute and impermeable reference intravascular tracer as shown Figure 8.9. The figure diagrams an experimental setup for examining the uptake of D-glucose in an isolated perfused heart as by Kuikka et al. (6). L-glucose, the stereo-isomer, serves as an extracellular, non-metabolized reference. A more realistic diagram of a capillary–tissue exchange includes the endothelial cells and interstitial fluid (ISF), as shown in Figure 8.10.
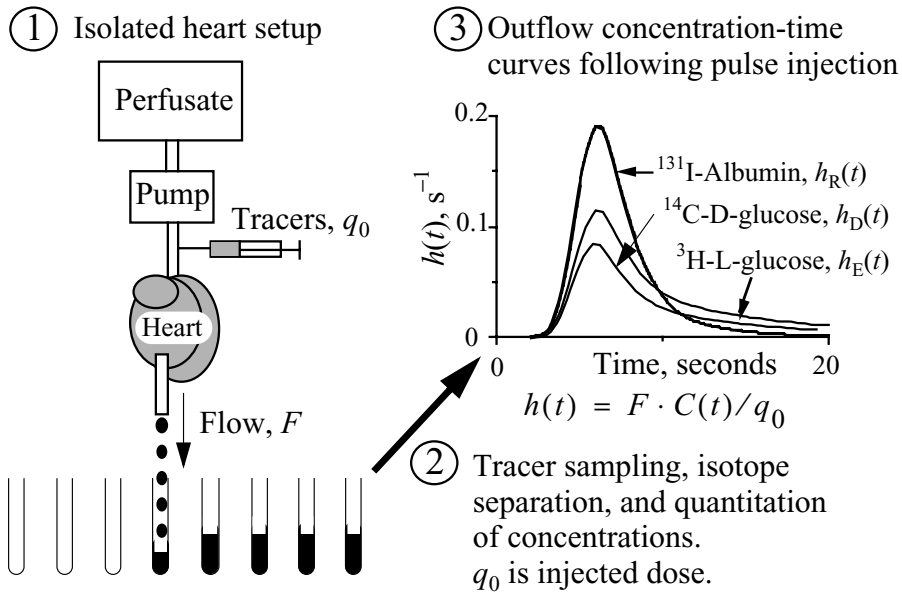
Figure 8.9. Schematic overview of experimental procedures underlying the application of the multiple-indicator dilution technique to the investigation of multiple substrates passing through an isolated organ without recirculation of tracer. The approach naturally extends also to their metabolites.

       To reduce this diagram to that of Figure 8.8 requires a further set of assumptions. For current purposes these are that the endothelial layer, the interstitial fluid space and the plasmalemma of the parenchymal cell can be represented by a single composite barrier, and ignores the capacitance of these structures.

       To determine capillary permeability the relevant reference solute is one that does not escape from the capillary blood during single transcapillary passage; for example, albumin is the relevant reference solute to determine the capillary permeability to glucose. In this situation the albumin dispersion along the vascular space may be assumed to be the same as that of the glucose; thus the shape of the albumin impulse response, $h_{alb}(t)$, accounts for the intravascular transport of all the solutes. (L-glucose, an extracellular reference tracer with the same molecular weight and diffusivity as D-glucose, is the extracellular reference for D-glucose, having the same capillary PS_c and the same interstitial volume of distribution, V_{isf}. Having simultaneous data on such reference tracers greatly reduces the degrees of freedom in estimating the parameters of interest for D-glucose.)

       An ideal set of reference solutes for evaluating a Figure 8.10 model is provided in Table 8.2. Fitting MID concentration-time curves for the first three classes of solutes with the model solutions provides estimates of the parameters listed in the right column, and approximates or even gives exactly the parameter values for the test substrate.

For the test substrate the observed data are fitted using only the few remaining free parameters for binding and reaction. To examine the effects of model reduction, we will use only the intravascular reference marker and the solute of interest which enters the parenchymal cell, of which V_2 in Figure 8.8 is the analog.

While we have fully developed mathematical models for the system diagrammed in Figure 8.10 (7, 8), including ones with facilitating transporters and sequences of reactions (9), our present purpose is satisfied by the simplest models that allow us to assess the accuracy of estimates of the permeability, PS, of the capillary barrier to a solute.
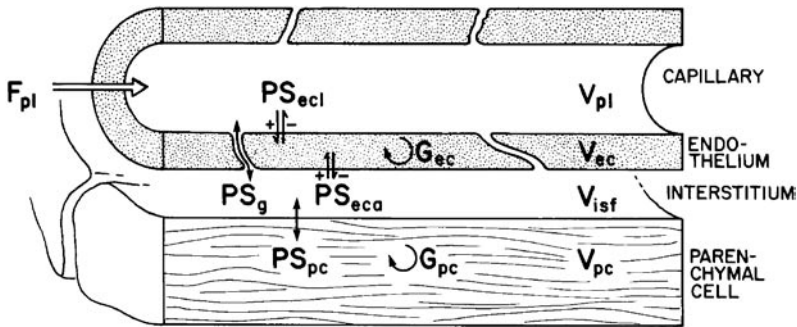

Figure 8.10. Representation of a blood-tissue model used for analysis of indicator-dilution curves. F, plasma (perfusate) flow, ml g^{-1} min^{-1}, PS, permeability-surface areas, ml g^{-1} min^{-1}, for passage through endothelial cell luminal membrane (PS$_{ecl}$); water-filled channels or gaps between endothelial cells (PS$_g$); endothelial cell albuminal membrane (PS$_{eca}$); and parenchymal cell membrane (PS$_{pc}$). G, intracellular consumption ml g^{-1} min^{-1} (metabolism) of solute by endothelial cells (G$_{ec}$) or by parenchymal cells (G$_{pc}$). V, ml g^{-1}, volume of plasma (V$_{plasma}$), endothelial cell (V$_{pc}$), interstitial (V$_{isf}$) and parenchymal cell (V$_{pc}$) spaces, the anatomic volumes, ml g^{-1}. (Figure from Gorman et al. (18) with permission from the American Physiological Society.)

Table 8.2. Reference tracers for a substrate

Solute Class	Example	Information provided by the solute class
Intravascular	Albumin	Convective delay and dispersion in all vessels perfused.
Extracellular	L-glucose	C$_{left}$ PS$_g$, and interstitial volume, V $_{isf}$
Unreacted but transported analog	3-O-methyl -D-Glucose	Cell PS$_{pc}$; intracellular volumes of distribution, V$_{pc}$ and V$_{ec}$
The test substrate	D-glucose	Binding space; reaction rates inside cells, G$_{ec}$, G$_{pc}$

Model Equations for Tracer:

The diagram in Figure 8.10 looks, and is, different from that of Figure 8.8, but with the assumptions listed above reduces to the same model. Capillaries are of the order of 1 mm long, and are 5 microns in diameter, an aspect ratio of 200. Diffusional relaxation times differ by a factor of 200 between radial and axial directions. Consequently, considering the capillary as a stirred tank is unreasonable. The stirred tank expressions, with no intravascular binding, are the same as Model 1B except for the addition of the flow through compartment 1, the consumption term G_2 ml g^{-1} s^{-1} to the second compartment, and the omission of binding from the first:

$$\frac{dC_1^*}{dt} = \frac{F}{V_1}\left(C_{in} - C_{out}\right) - \frac{PS}{V_1}\left(C_1^* - C_2^*\right) \qquad [21]$$

$$\frac{dC_2^*}{dt} = \frac{PS}{V_2}\left(C_1^* - C_2^*\right) - \frac{G_2}{V_2}\cdot C_2^* \qquad [22]$$

The use of these ODEs implies and builds into the calculations a discontinuity between the concentration of solute in the inflow and that in V_1. Because V_1 is assumed instantly mixed, there is no gradient along the capillary and the tracer entering the tank is immediately available to be washed out with the same probability as any molecule dwelling in there for a longer time.

    Alternatively the capillary-tissue unit of Figure 8.10 can be reduced to two regions represented by partial differential equations (PDEs) that allow a continuous gradient along the path between entrance and exit. Using the spatially distributed analogs for plasma, C_p, or blood, and extravascular tissue, C_{tiss}, to represent the lumped variables C_1 and C_2:

$$\frac{\partial C_p(x,t)}{\partial t} = -\frac{F_p L}{V_p}\cdot\frac{\partial C_p}{\partial x} - \frac{PS_C}{V_p}\left(C_p - C_{tiss}\right) + D_p\frac{\partial^2 C_p}{\partial x^2} \qquad [23]$$

$$\frac{\partial C_{tiss}(x,t)}{\partial t} = -\frac{PS_C}{V_{tiss}'}\left(C_{tiss} - C_p\right) - \frac{G_{tiss}}{V_{tiss}'}C_{tiss} + D_{tiss}\frac{\partial^2 C_{tiss}}{\partial x^2} \qquad [24]$$

where C_p and C_{tiss} are spatially distributed functions of both x and t, not just t. The axial position is denoted by x, where $0 < x < L$, the capillary length, cm. The analogy between this model and the compartmental version in Eqs. [21] and [22] is $F_p = F$, $V_p = V_1$, $V_{tiss} = V_2$, and $PS_c = PS$, the permeability-surface area of the capillary wall, but we retain the two sets of names in order to make comparisons between the estimated parameter values. The capillary length is arbitrarily set to an average value such as 0.1 cm. PDEs require boundary conditions: at the capillary entrance, $C_p(x=0, t) = C_{in}$, so there is no discontinuity in the concentration profile; at the exit $C_{out} = C_p(x=L, t)$, as a result of the no-flux boundary condition and the same condition described by the ODEs.

The last term in each equation is the diffusion along the length of the capillary-tissue regions; the use of an anatomically correct length then makes using observed diffusion coefficients for D_p and D_{tiss}, cm^2 s^{-1}, practical and meaningful. Gross exaggeration of the diffusion coefficients can be used in the equations to turn the distributed model into a *de facto* well-mixed, compartmental model.

The flow term merits further explanation since it might appear that the sign in the first right-hand side term of Eq. [23] differs from that of Eq. [21]. Consider the inflow to contain a bolus of solute: as it enters, the concentration at the capillary entrance rises. At this time, the slope of the curve of concentration versus position x, $\partial C/\partial x$, is negative as illustrated by the slope of C(x,t) for the bolus shape at t=1.5s, at the capillary mid point, x=0.5 L. The spatial slope has always the sign opposite to the temporal derivative $\partial C/\partial t$ at the same point, thus the negative sign on the term.

Functionally, therefore Eqs. [23] and [24] are analogous to Eqs. [21] and [22]. But using the PDEs avoids the unrealistic discontinuity in the compartmental model at the entrance, which is the corollary to the instantaneous mixing within V_1. Most important, the PDE allows continuity in concentrations and concentration gradients along the capillary, and not only in concentration but also in the properties of the system such as axial gradients in transporter and enzyme densities that are evident in the liver sinusoid. For the following analysis, all parameters are assumed spatially uniform so as to minimize the difference from the compartmental models. There are many ways of representing axially distributed convecting systems, and two are shown in Figure 8.11A. The usual approaches solve the PDE using one of several PDE solvers (10), and here we used a Lagrangian method (8). A compartmental type of alternative is to approximate the capillary as a series of stirred tanks, each with the same volume and PS. With a large number of serial stirred tanks, the longitudinal concentration gradient is approximated accurately as the steps from one to the next are small. The intravascular transport process with serial stirred tanks is a Poisson process. In modeling, serial stirred tanks are convenient because the number of tanks can be used as a free parameter. The relative dispersion over the length of the tube is determined by N_{tanks} such that the relative dispersion RD, which equals the coefficient of variation, induced during transit is $1/\sqrt{N_{tanks}}$, so that with 100 tanks the RD is 10%.

Figure 8.11A shows that curves for the PDE solution and for the Poisson process are essentially similar, so that the dispersion coefficient D_p sufficed to create the same dispersion as occurred with the Poisson process using 109 tanks. The choice of 109 tanks is arbitrary: so large that a plot of C(N_{tanks}) versus N would appear smooth. The permeative loss is the same for both methods, with the result that the peak outflow concentrations are similar. Figure 8.11B shows the shape of the bolus as a function of position as it deforms continuously from its initial square pulse at the entrance to the capillary. Because the capillary PS > 0, there is loss of solute as the bolus progresses along the capillary. The diminution in peak height is therefore due not only to the spreading but to the loss. This loss is reflected of course in the reduction in the areas
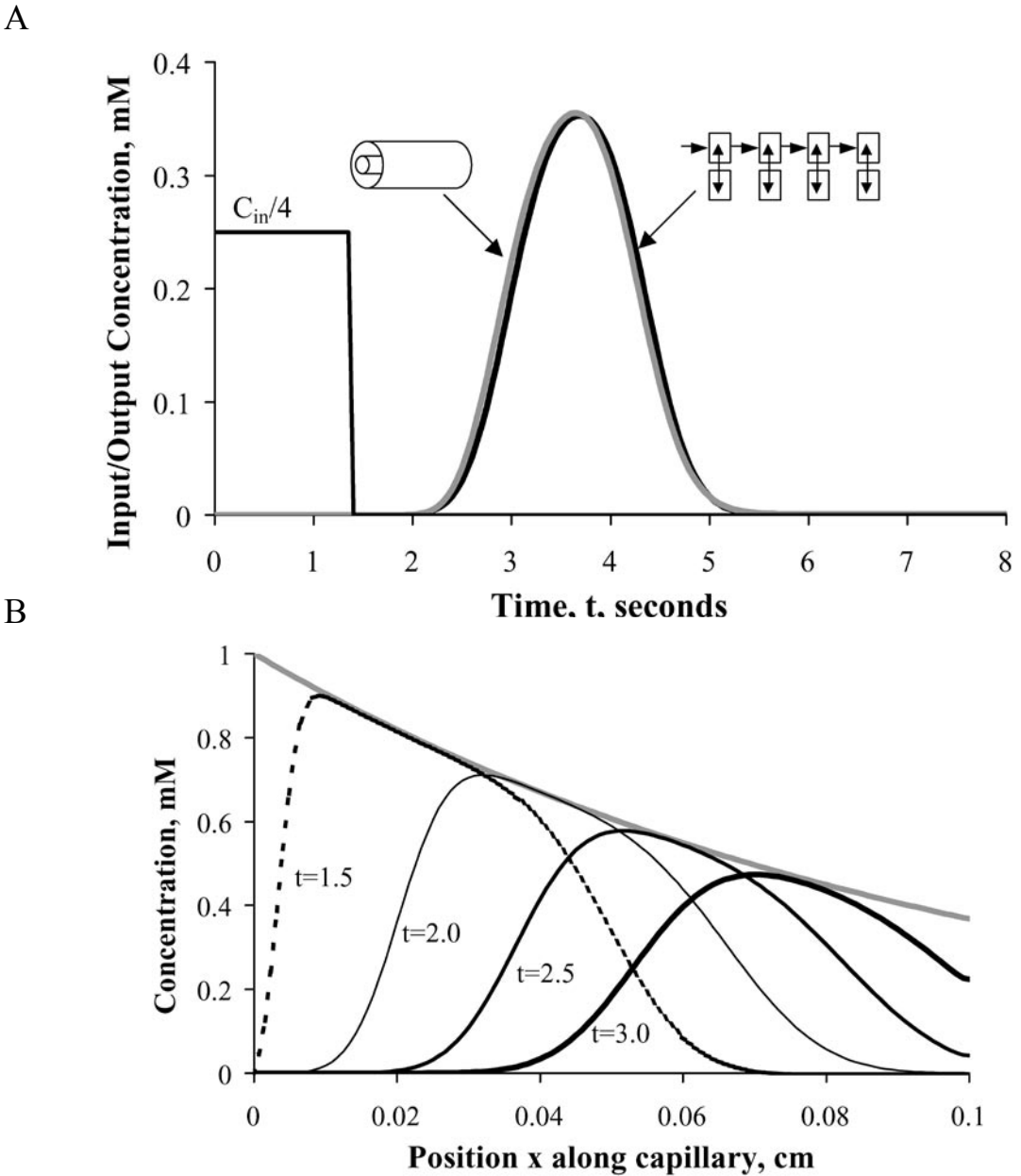
A

B

Figure 8.11. Pulse responses in axially-distributed models. The input function, C_{in}, is a pulse of duration 1.4 seconds. Panel A: Outflow concentration-time curves for a PDE solution using a Lagrangian sliding fluid element method and an intravascular dispersion coefficient, $D_p = 2.6 \times 10^{-5}$ cm^2 s^{-1} (gray curve), and for a serial stirred tank algorithm representing a Poisson process with 109 stirred tanks (black curve almost superimposed on the gray one). Panel B: Intracapillary spatial profiles at a succession of times, 1.5, 2.0, 2.5, and 3.0 seconds, as the pulse propagates and disperses while some of the solute permeates the capillary wall. Parameters were the same for the Poisson model and the PDE: $F_p = 1$ ml g^{-1} min^{-1}, $PS_C = 2$ ml g^{-1} min^{-1}, and tissue volume V_{tiss} was set to 10 ml g^{-1} so that there was negligible tracer flux from tissue back into the plasma space.

under the successive plots of $C_p(t, x)$ as solute escape into the extravascular region. (For this illustration the value of V_{isf} is set so abnormally high (10 ml g^{-1}) that C_{isf} remains negligible and there is no back flux from ISF to plasma.)

While the Poisson operator with a large number for N_{tanks} can be used to fit data, it is computationally less efficient than solving the PDE directly, and the additional disadvantage that the dispersion cannot be controlled independently of choosing N_{tanks}. The relative dispersion with $N_{tanks} = 10$ is 0.318 ($= \sqrt{10}/10$), and with $N_{tanks} = 1$ is 1.0. While finite element grids for solving the PDEs can be rather coarse, e.g. 10 to 20 grid segments, in contrast when using the serial compartments, N_{tanks} must remain high to recover curves that resemble those of the experimentally observed curves. Figure 8.12 illustrates the dramatic shape changes brought about by reduction of N_{tanks}. All of the Poisson operator outputs in the figure have mean transit times identical to that of the gray reference PDE curve. The solutions using low N_{tanks} have excessively long low tails to balance the too early peaks.

Fitting data with the model functions.
We chose as an example a set of indicator dilution curves to which fitting a 3-region model is required, namely the uptake of adenosine in the heart wherein the endothelial cell metabolism is neglected and the capillary wall is considered as one membrane to cross, and thereby ignoring endothelial capacitance and reactions. The three regions are capillary plasma, ISF, and parenchymal cell, using the terminology of Figure 8.10, and the equations are Eqs. [23] and [24], the latter being for the ISF, and then adding a similar equation for the parenchymal cell and accounting for exchanges between ISF and parenchymal cell. (The 3-region model and the Lagrangian sliding fluid element method of solution have been described (8).) Figure 8.13 shows model fits to the three simultaneously obtained experimental curves. The Lagrangian PDE solutions for the three cases are essentially identical to the serial stirred tank model solutions (not shown), using identical values for all of the physiological parameters, the flows, volumes, permeabilities, and consumption in the parenchymal cell, G_{pc}. The value for G_{pc} was set to a high value for this illustration and was not optimized, in accord with the fact that almost no tracer adenosine returns from the cell to the effluent plasma. The point of Figure 8.13 is that so long as the models account appropriately for the intracapillary concentration gradients, the three anatomic volumes, the observed flow, and intravascular dispersion, then the estimates of permeabilities are the same from the two models. When volumes and flows are the same then, by mass conservation, the mean transit times are forced to be the same.

However if the representation of the convective region is compromised by using fewer compartments, errors must be introduced into other parameters in order to fit the data. Figure 8.14 shows that the model solution can be obtained to fit the albumin data even with N_{tanks} as low as 15. Achieving such a result with $N_{tanks} = 15$ is implicit with the method used here and has no scientific value; because no data on the
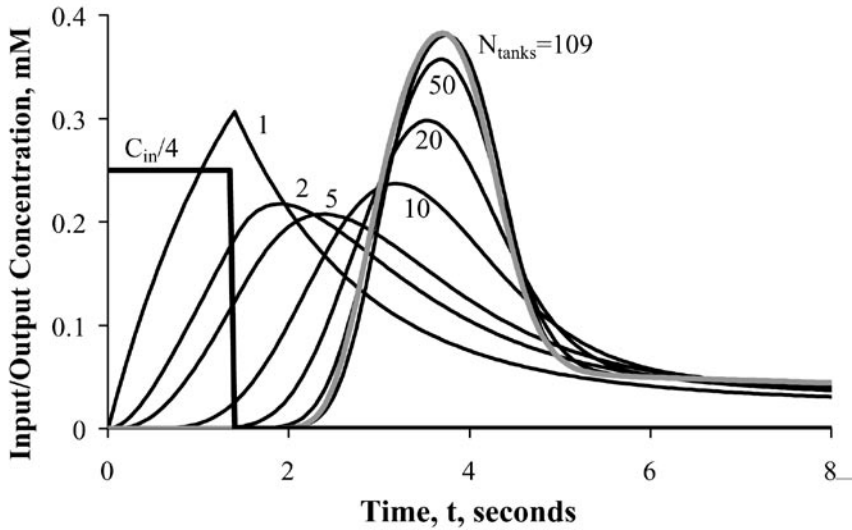
Figure 8.12. Responses of the Nth order Poisson operator with N_{tanks} varied from 109 tanks in series down to 50, 20, 10, 5, 2, and finally to a single mixing chamber, $N_{tanks} = 1$. The gray curve is the Lagrangian solution to the PDEs as in Figure 8.11. All of the Poisson operator outflow curves (black) have the same mean transit time, but differ in their shapes. The parameters were $V_p = 0.05$ and $V_{tiss} = 0.15$ ml g^{-1}; $F_p = 1$ ml g^{-1} min^{-1}, $PS_C = 1$ ml g^{-1} min^{-1}.
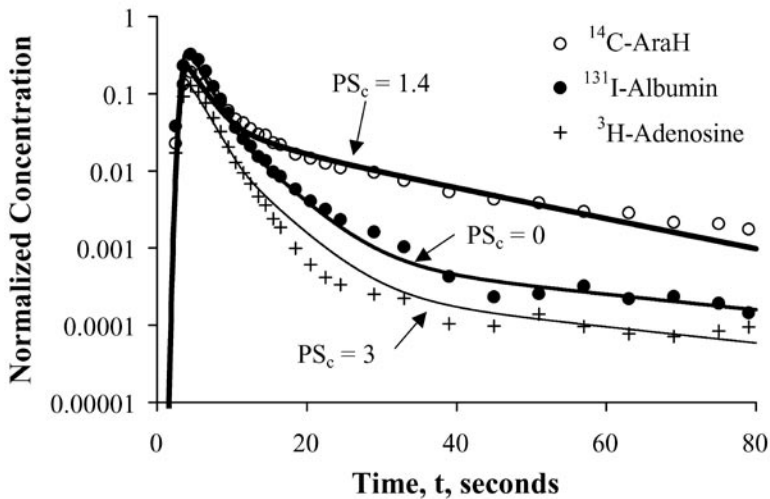

Figure 8.13. Multiple indicator dilution experimental curves fitted simultaneously with three-region PDE (shown) and serial compartmental models, using $N_{tanks} = 80$ for the latter (not shown but identical to PDE solution for long times). The parameters were $V_p = 0.1$ and $V_{isf} = 0.4$ ml g^{-1}; $F_p = 2.8$ ml g^{-1} min^{-1} (experimental value); $PS_C = 0.019$ ml g^{-1} min^{-1}, for albumin, 1.3 for AraH, and 3.0 for adenosine; $PS_{pc} = 25$ ml g^{-1} min^{-1} and $G_{pc} = 10^4$ ml g^{-1} min^{-1} for adenosine (both zero for other tracers) and $V_{pc} = 0.55$ ml g^{-1}. Data from Schwartz et al. (11).
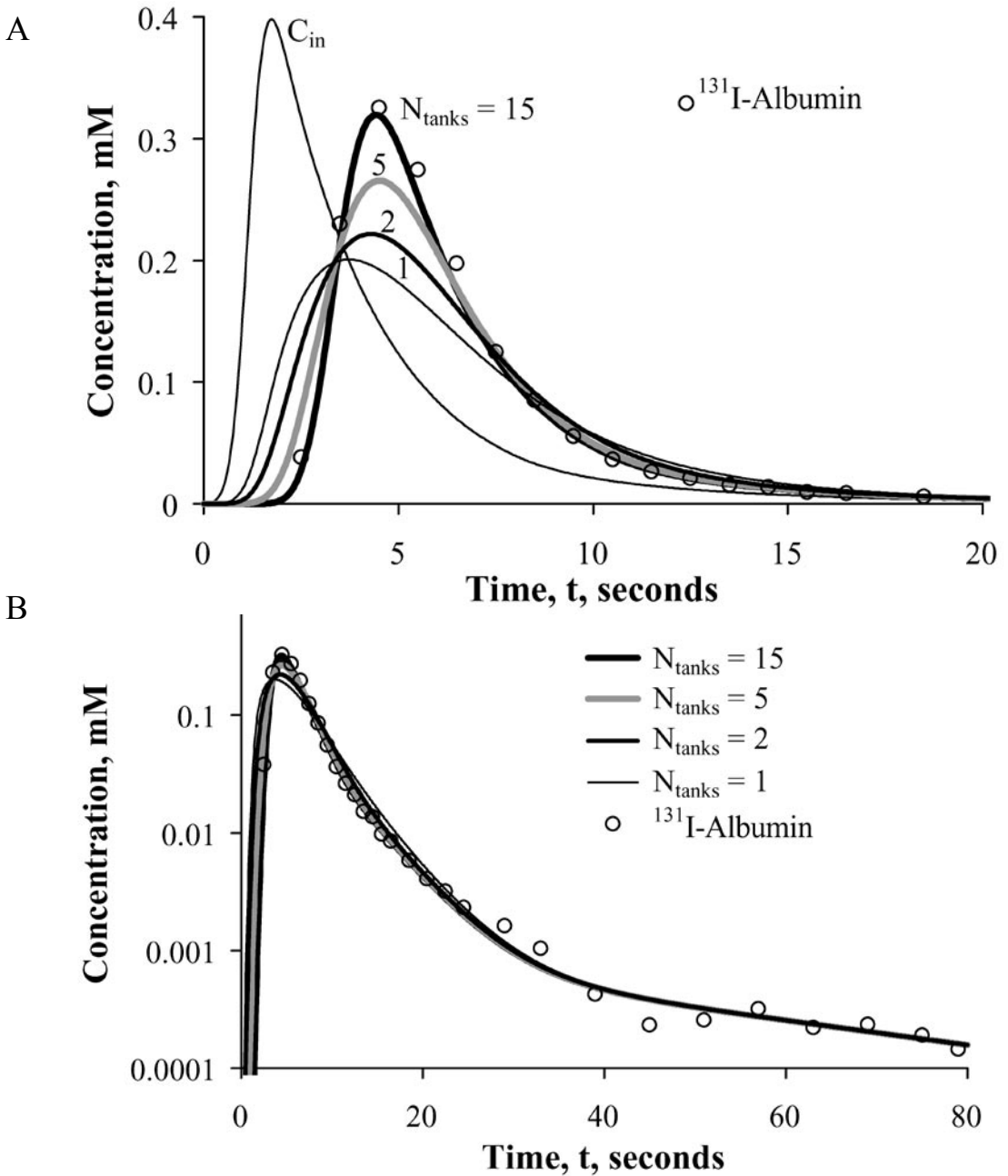
Figure 8.14. Fitting the intravascular reference ^{131}I-Albumin curve with the serial stirred tank model with N_{tanks} = 15 gives a good fit. Panel A: Linear plot showing the first 20 seconds of the transients. Using fewer compartments N_{tanks} = 5, 2, and 1, results in outflow concentration time curves that do not fit the experimental data, the model curves being too low peaked and too dispersed in time. Panel B: Semilogarithmic plot to show the whole data set (to 80 seconds). The failure to fit the upslope and peak of the curve which is obvious in the top panel is less apparent (though it is exactly the same) but the tail of the albumin curve is fitted well by all of the models.

input function were available, an input function of arbitrary form was constructed by an iterative procedure (in effect a deconvolution) until the output at the known flow fitted the albumin curve, so the satisfactory fit is merely self-fulfilling. If one wishes to fit the data with $N_{tanks} < 15$, then a new input function must be estimated so as to fit the albumin curve. This works for any number of tanks, illustrating that the choice of a model to fit the data is completely arbitrary and has no relation to the reality of the choice of a compartmental model. The corollary is that the anatomic and physiological parameters will be estimated erroneously. To avoid this problem, the real input function should be recorded during the experiment, thus avoiding the need for a deconvolution.

Since it is often difficult experimentally to record the input function, this is a common predicament. What is demanded however, is that in order to elicit parametric information at the capillary-tissue exchange level, one must use the *same* input function for the whole set of data curves, e.g. the set in Figure 8.13. The failure of compartmental analysis is exemplified by the results shown in Figure 8.15 with the same data set as in Figure 8.13. In Figure 8.15A, which uses $N_{tanks} = 15$, the parameters are almost the same as estimated using the PDE solution (Figure 8.13) or using $N_{tanks} = 109$. However, with $N_{tanks} = 1$ (Figure 8.15B), the parameters are systematically different (Table 8.3): overestimating PS_C at 20 compared to 3 and underestimating PS_{pc} at 7 compared to 20 ml g^{-1} min^{-1}. G_{pc} is only modestly underestimated at 60 compared to 90 ml g^{-1} min^{-1}. The interstitial volume, V_{isf}, is also underestimated at 0.20 ml g^{-1} compared to 0.33 to 0.4 ml g^{-1}. While for $N_{tanks} = 1$ (Figure 8.15B) the input function allowed a good fit to the first 20 seconds of the curves, the tails could not be closely fitted. The single tank convective region forces the tail to become monoexponential earlier than is seen for the more spatially distributed models. (They all become monoexponential eventually.) Table 8.3 shows the results for other values of N_{tanks}, where it can be seen that the estimates tend to deviate in a systematic fashion as N_{tanks} diminishes. As N_{tanks} diminishes from 15 to 5, 2, and 1, the estimate of PS_C rises 6 fold, PS_{pc} diminishes 30% for AraH and 70% for Ado, V_{isf} for AraH by 35%, V_{pc} rises 40% for AraH, and G_{pc} for Ado falls 30%.

The inference is clear. Given that one has trust in the physically realistic PDE version of the physical situation, constrained as it is by using values for the regional volumes taken from the anatomy, then the compartmental models systematically and progressively deviate from the physiological values even though the curves can be fitted not too badly. In no case did single stirred tank models fit well ($N_{tanks} = 1$, Figure 8.15B), but for larger values of N_{tanks} the fits were quite good. Now it is obvious that getting a good fit to the selected tracer dilution curves alone fails to guarantee sensible results. In every study there are other data, usually ignored, such as the anatomy, other known physiological features, ionic or transmembrane charges, pH, previously identified reactions, binding sites and so on, that should be used in the analysis. When these "knowns" are incorporated into the scheme, and the basic conservation rules applied, then one starts to get physiologically valuable parameters and an understanding of the system.
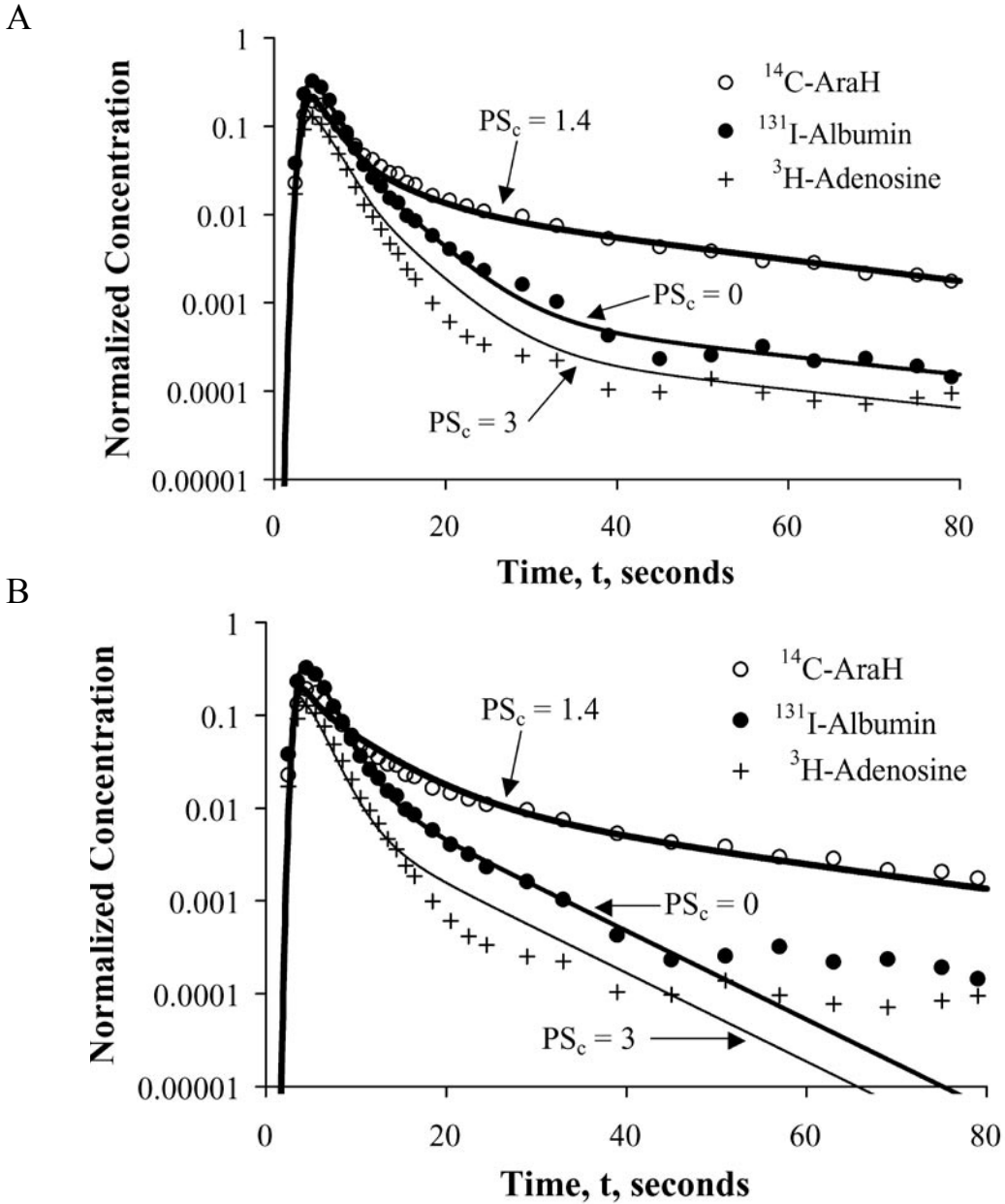
A

B

Figure 8.15. MID curves for ^{131}I-Albumin, ^{14}C-AraH, and ^{3}H-Adenosine fitted using the serial tank model and a common input function. Panel A: $N_{tanks} = 15$ as in Figure 8.14. Curves fitted almost as well as with the PDEs used in Figure 8.13. Parameters for the adenosine curve were $F_p = 2.8$ (experimental data), $PS_C = 3$, $PS_{pc} = 20$, and $G_{pc} = 90$ ml g^{-1} min^{-1}, with $V_p = 0.11$, $V_{isf} = 0.33$ and $V_{pc} = 0.55$ ml g^{-1}. Panel B: $N_{tanks} = 1$. The albumin curve is well fitted, but the input function differs from that used in the top panel. Parameters for the adenosine curve were $PS_C = 3$, $PS_{pc} = 7$, and $G_{pc} = 60$ ml g^{-1} min^{-1}, with $V_p = 0.10$, $V_{isf} = 0.20$ and $V_{pc} = 0.55$ ml g^{-1}.

To get closer to reality, the models have to be more complex. For example, the capillary wall is tiled with endothelial cells with transport occurring through interendothelial clefts and across the endothelial cell bodies, so PS_C actually represents a sum of two conductances in parallel, a transendothelial facilitated transport process and passive diffusion through the interendothelial cleft [11]; to account for this in the analysis, the more complex model (of the form shown in Figure 8.10) is used to account separately for cleft permeation and transendothelial flux.

Table 8.3 Parameter Estimates at differing N_{tanks}

Species	$N_{tanks}=$	15	5	2	1
	PS_c, ml g^{-1} min^{-1}	1.4	1.3	2	8
	PS_{pc}, ml g^{-1} min^{-1}	1	0.85	0.65	0.7
^{14}C-AraH	V_{isf}, ml g^{-1}	0.33	0.3	0.28	0.2
	V_{pc}, ml g^{-1}	0.2	0.22	0.25	0.28
	PS_c, ml g^{-1} min^{-1}	3	3	5	20
^{3}H-Adenosine	PS_{pc}, ml g^{-1} min^{-1}	20	20	9	7
	V_{pc}, ml g^{-1}	0.55	0.55	0.55	0.55
	G_{pc}, ml g^{-1} min^{-1}	90	70	70	60

No free parameters were used for fitting the Albumin curve.

For the adenosine (Ado) analysis V_{pc} was fixed at 0.55 ml g^{-1}, and not optimized.

All other parameters were estimated from the data.

Discussion

Metabolic events within cells are intimately linked with the external influences of substrate delivery and metabolite removal. These influences include the rates of transport by blood flow and transmembrane processes as well as the regulation of enzymatic reactions. Further influences include intravascular and intracellular binding, where one finds the influences discussed in Section I. An obvious example is that the transport of respiratory gases through the circulation is dominated by their binding and buffering in the blood, which in turn influence their rates of delivery and exchange. In Section I we showed that errors in parameterization occur when the assumption of instantaneous binding is incorrect. A second inference is that parameter values obtained during steady state cannot be expected to have validity during a changing state, nor in a subsequent steady state where concentrations differ from those in the initial steady state.

Solute binding is common for pharmacologic agents, hormones, vitamins, and the body's normal constituents like fatty acids. In fact one can generalize by saying that most lipid soluble substances are carried in sequestered or bound form in the blood and that their fluxes into tissues and cells are facilitated by transporter proteins. The fact

that most drugs and hormones are also bound to blood components, e.g. retinone, fatty acids, either RBC or plasma proteins, invites consideration of the similarity between the mechanisms of their exchanges and those of oxygen. Further, most drugs and solutes of interest are less soluble in membranes than is oxygen (whose transport across lipid membrane is so fast as to be limited solely by delivery to the membrane surface, not by the permeation process itself), and commonly require specialized transporters to facilitate transfer. Where transporters are required, there is virtually always competition for the binding sites, so transport rates for a foreign drug or a tracer-labeled solute can be expected to be somewhat dependent on the ambient concentrations of those native solutes or other drugs.

In Section II the emphasis is not merely a comparison of the efficacy of distributed versus compartmental models, but on the critical need to incorporate what is known about a system into the analysis. Accounting for the anatomy is as important as obeying conservation requirements. In general one needs to adhere to the constraints provided by prior studies, the anatomy being primary since it is usually well defined. Anatomy is accounted for by using PDEs in capillary-tissue exchange processes. Failure to use anatomic information and to seek the simplicity of "minimal models" sacrifices the reality of estimates of the primary physiological parameters, particularly those like the permeability-surface area products, which dominate the kinetics. For example, in blood-perfused tissues the calculation of the axial intracapillary oxygen profiles is more complex because of oxygen binding to hemoglobin, Hb, and the influences of carbon dioxide, pH, and temperature, all of which have intracapillary gradients, on the oxygen binding. Axial gradients in P_{O_2} are more linear than exponential (12).

Single compartmental analysis gives estimates of model parameters up to several-fold different from those emerging from high resolution analysis using the PDEs to conform to anatomic constraints. Qualitative compartmental modeling is certainly useful for categorization or classification. When the compartmental mixing assumption is valid, physical or physiological parameters can be correctly estimated. This essay is an attempt to stimulate each modeler's curiosity and thoughtful assessment of the applicability of stirred tank approximations.

Initially, compartmental analysis was used because computational power was relatively low but the implicit compromise was inaccurate estimation of the physiological parameter values. Currently, computer power is less of an issue and models can be fully specified and accurately computed using algorithmically efficient PDE solvers. Other approaches to gaining speed involve a reduction in the number of free parameters such as in an optimization procedure where using known values for volumes of distribution or known K_m's for enzymatic reactions or transporters are used. Additional efficiency can be gained by using thermodynamic constraints (e.g., Haldane constraints in biochemical networks (13) to limit parameter ranges (14).

These considerations for modeling the physiology with high fidelity while minimizing computational effort can be facilitated by following a set of guidelines for

developing the models. The primary recommendations for the modeling of biological systems are the following:

1. **Use the known anatomy, structure, and composition to constrain estimates** of local and overall volumes of distribution, routes of transport, and other kinetic possibilities. These are not necessarily measured in every experiment, but in general should be considered as parts of the experimental data since their means and standard deviations are known and they provide realistic constraints. For example, the water fraction of heart muscle is so narrowly constrained that it can be used as a constant, being 0.78 +/- 0.01 ml g^{-1} tissue (15), and is used to constrain the estimates of intracellular and intramitochondrial concentrations of ATP (16).

2. **Define parameters and variables in physiologically meaningful terms** in order to stimulate re-examination of assumptions at each stage. Consider the details of the underlying physiology in defining the model in order to constrain its form and behavior. For example, use continuity in concentration profiles along segments of the vascular system or within cells. In using mathematics that describes the biology, don't compromise the mathematics to fit limitations in computational methods, but compromise later, with caution. Use standardized terminology (17) where possible, and try to use terms defined in ontologies such as the Foundations of Medical Anatomy in order to maintain uniqueness of terms.

3. **Apply conservation principles (mass, charge, volume, energy)**, and relevance to a viable steady state, preferably checking for these in each program. Provide thermodynamic constraints on all reactions. Provide units for all variables and parameters. Use technology which automatically checks for unit balances and thereby forces identification of errors.

4. **Recognize that the fundamental description of the kinetics of tracers is always at the molecular level,** therefore "think like a molecule" on how each process occurs: Convected in the blood in a bound or free state? How is the membrane traversed? How does each reaction occur, and where? The tenet of tracer methods is not that the system should be in steady state, but that the linearized coefficients for the tracer kinetics are slaved to the fluxes for the tracee in both transient and steady states. Use dual models, tracee and tracer, where the tracee model contains all the physiological mechanisms, while the tracer model has its coefficients directly derived from the current ambient state for tracee.

5. **Adhere to standard requirements** for the design, performance, documentation, and dissemination of models. The goal in presenting a model is easy and accurate reproducibility by a user community of researchers, teachers, and students.

Standards for documenting and archiving a model are being developed, and a preliminary version can be found at www.physiome.org/Models/standards.html. Whenever such standards are not being met, think of it as an invitation to explain that something is missing or assumed in the modeling. It is probable that journals will establish such criteria for publication. Certainly the federal funding agencies are moving rapidly toward requiring that the results of federally funded research be made publicly available.

Acknowledgements

Correspondences

Please address all correspondence to:

James B. Bassingthwaighte, M.D., Ph.D.
University of Washington, Box 355061
Dept. of Bioengineering
Seattle, WA 98195-5061
Phone: 206-685-2005
Fax: 206-685-3300
Email: jbb@bioeng.washington.edu

References

1.   Berman M. The formulation and testing of models. Ann N Y Acad Sci. 1963 May 10;108:182-94.

2.   Krogh A. The number and distribution of capillaries in muscles with calculations of the oxygen pressure head necessary for supplying the tissue. J Physiol. 1919 May 20;52:409-15.

3.   Cobelli C, Foster D, Toffolo G. Compartmental versus noncompartmental kinetic parameters. Tracer Kinetics in Biomedical research From data to model. New York: Kluwer Academic; 2002. p. 191-213.

4.   Chinard FP, Vosburgh GJ, Enns T. Transcapillary exchange of water and of other substances in certain organs of the dog. Am J Physiol. 1955 Nov;183:221-34.

5.   Crone C. The Permeability of Capillaries in Various Organs as Determined by Use of the 'Indicator Diffusion' Method. Acta Physiol Scand. 1963 Aug;58:292-305.

6.   Kuikka J, Levin M, Bassingthwaighte JB. Multiple tracer dilution estimates of D- and 2-deoxy-D-glucose uptake by the heart. Am J Physiol. 1986 Jan;250: H29-42.

7.   Bassingthwaighte JB, Wang CY, Chan IS. Blood-tissue exchange via transport and transformation by capillary endothelial cells. Circ Res. 1989 Oct;65:997-1020.

8.   Bassingthwaighte JB, Chan IS, Wang CY. Computationally efficient algorithms for convection-permeation-diffusion models for blood-tissue exchange. Ann Biomed Eng. 1992;20:687-725.

9.   Bassingthwaighte JB, Raymond GM, Ploger JD, Schwartz LM, Bukowski TR. GENTEX, a general multiscale model for in vivo tissue exchanges and intraorgan metabolism. Philos Transact A Math Phys Eng Sci. 2006 Jun 15;364:1423-42.

10.   Poulain CA, Finlayson BA, Bassingthwaighte JB. Efficient numerical methods for nonlinear-facilitated transport and exchange in a blood-tissue exchange unit. Ann Biomed Eng. 1997 May-Jun;25:547-64.

11.   Schwartz LM, Bukowski TR, Ploger JD, Bassingthwaighte JB. Endothelial adenosine transporter characterization in perfused guinea pig hearts. Am J Physiol Heart Circ Physiol. 2000 Oct;279:H1502-11.

12. Dash RK, Bassingthwaighte JB. Simultaneous blood-tissue exchange of oxygen, carbon dioxide, bicarbonate, and hydrogen ion. Ann Biomed Eng. 2006 Jul;34:1129-48.

13. Vinnakota K, Kemp ML, Kushmerick MJ. Dynamics of muscle glycogenolysis modeled with pH time course computation and pH-dependent reaction equilibria and enzyme kinetics. Biophys J. 2006 Aug 15;91:1264-87.

14. Beard DA, Liang SD, Qian H. Energy balance for analysis of complex metabolic networks. Biophys J. 2002 Jul;83:79-86.

15. Yipintsoi T, Scanlon PD, Bassingthwaighte JB. Density and water content of dog ventricular myocardium. Proc Soc Exp Biol Med. 1972 Dec;141:1032-5.

16. Vinnakota KC, Bassingthwaighte JB. Myocardial density and composition: a basis for calculating intracellular metabolite concentrations. Am J Physiol Heart Circ Physiol. 2004 May;286:H1742-9.

17. Bassingthwaighte JB, Chinard FP, Crone C, Goresky CA, Lassen NA, Reneman RS, Zierler KL. Terminology for mass transport and exchange. Am J Physiol. 1986 Apr;250:H539-45.

18. Gorman MW, Bassingthwaighte JB, Olsson RA, Sparks HV. Endothelial cell uptake of adenosine in canine skeletal muscle. Am J Physiol. 1986 Mar;250:H482-9.